nature reviews earth & environment

https://doi.org/10.1038/s43017-025-00705-7

Review article

Check for updates

Climate impacts of the El Niño–Southern Oscillation in Africa

Wenju Cai[1,2,3] ✉, Chris Reason[4], Elsa Mohino[5], Belen Rodríguez-Fonseca[5,6], Johan Malherbe[7], Agus Santoso[8,9] ✉, Xichen Li[10,11], Hector Chikoore[12], Hyacinth Nnamchi[13,14], Michael J. McPhaden[15], Noel Keenlyside[16,17,18,19], Andrea S. Taschetto[9,20,21], Lixin Wu[1,3], Benjamin Ng[22], Yi Liu[1], Tao Geng[3], Kai Yang[22], Guojian Wang[22], Fan Jia[3,23], Xiaopei Lin[1,3], Shujun Li[1,3], Yun Yang[24], Junkai Wang[1], Li Zhang[1,3], Ziguang Li[1], Pokam Wilfried[25], Liming Zhou[26], Xuebin Zhang[22], Francois Engelbrecht[27], Zhuoran Li[28] & Joseph N. Mutemi[29]

Abstract

The El Niño–Southern Oscillation (ENSO) — describing shifts between warm El Niño and cold La Niña phases — has a substantial effect on the global climate. In this Review, we outline the mechanisms and climate impacts of ENSO in Africa, focusing on rainfall. ENSO's influence varies strongly by season, region, phase, event and decade, highlighting complex dynamics and asymmetries. Although difficult to generalize, key characteristics include: anomalies across the Sahel in July–September, related to the tropospheric temperature mechanism; a strong dipole in anomalies between eastern and southern Africa during October–December (the short rain reason) and December–February, linked to interactions with the Indian Ocean Dipole and Indian Ocean Basin mode, respectively; and anomalies over southern Africa (with possible indications of opposite anomalies over East Africa) during March–May (the long rain season), associated with continuation of the Indian Ocean Basin mode. These teleconnections tend to be most pronounced for East Pacific El Niño and Central Pacific La Niña events, as well as during decades when interbasin interactions are strongest. Although challenging to simulate, climate models suggest that these impacts will strengthen in the future, manifesting as an increased frequency of ENSO-related dry and wet extremes. Given the reliance of much of Africa on rain-fed agriculture, resolving these relationships is vital, necessitating realistic simulation of regional circulations, ENSO and its interbasin interactions.

Sections

A full list of affiliations appears at the end of the paper. ✉e-mail: cwjresearch@gmail.com; Agus.Santoso@clivar.org

Introduction

Across Africa, hundreds of millions of people depend on seasonal rainfall for food security. This rainfall shows substantial geographical variability owing to features of the general circulation (Box 1): an arid climate prevails in the Sahara; semi-arid conditions in the Sahel, Greater Horn of Africa and parts of southern Africa; a monsoonal climate in parts of West Africa, East Africa and Madagascar; and a tropical climate in much of East Africa. Beyond such climatological differences are year-to-year rainfall fluctuations, often linked to modes of climate variability. For instance, the Indian Ocean Dipole[1,2] (IOD), the Indian Ocean Basin[3] (IOB) mode and the Atlantic Niño/Niña[4] are known to drive interannual changes in rainfall spanning the African continent.

Also of marked importance is the El Niño–Southern Oscillation (ENSO). Warmer-than-average sea surface temperatures (SSTs) in the eastern and central tropical Pacific — El Niño conditions — and cooler-than-average SSTs in the eastern and central tropical Pacific — La Niña conditions — both have global teleconnections that modulate African rainfall via interactions with other modes of variability[5,6], neighbouring oceans[4,7,8] and local circulation features[9–13]. Indeed, ENSO is known to have had a role in several catastrophic drought and flood events across the continent: the strong 1997 El Niño in driving floods in East Africa[14,15]; the strong 2015/16 El Niño in intense drought in southern Africa; the 2019 El Niño in floods in Uganda, Kenya, Ethiopia and Somalia; the consecutive 2020–2022 La Niña in drought spanning southern Ethiopia, southern Somalia and eastern Kenya; and the 2023/24 El Niño in simultaneous drought in southern Africa and extensive flooding in East Africa.

Given the reliance on rain-fed agriculture, each of these events had substantial societal impacts. For example, the 2015/16 El Niño and subsequent 2016/17 La Niña led to food shortages for an estimated 5–6 million people in southern Africa and across Kenya, Somalia and Ethiopia[16]. Similarly, the three-year La Niña-related drought in 2020–2023 contributed to food shortages for tens of millions and displacement of 3.3 million across Somalia, Ethiopia and Kenya[17]. These impacts highlight the importance of understanding ENSO–rainfall relationships in Africa, essential for accurate prediction and implementation of preparation measures to reduce socioeconomic consequences. At present, however, the complexity of ENSO–rainfall responses challenges such efforts, as seen during the 1997 and 2016 El Nino events, which had vast socioeconomic impacts.

In this Review, we assess the current knowledge of ENSO impacts on Africa, focusing on rainfall. We begin by describing the mechanisms by which ENSO affects Africa, including via interactions with the Indian and Atlantic Oceans, and modulation by extratropical processes and regional circulations. We subsequently outline its impact on the African climate, detailing the symmetrical responses, asymmetrical responses and multidecadal fluctuations. We next discuss challenges in modelling ENSO impacts and in projecting their changes under greenhouse warming. The Review ends by identifying pathways for progress.

Dynamical connections of ENSO to Africa

Various mechanisms govern ENSO impacts on the African climate. These mechanisms include tropical planetary-wave propagation, and interbasin interactions with the Indian and Atlantic Oceans that, in turn, influence atmospheric circulation over Africa, both of which are also modulated by extratropical processes and regional circulations. These aspects are now discussed, focusing on the linear dynamics associated with a typical El Niño; the dynamics of La Niña are assumed to be linearly opposite.

The tropical tropospheric temperature

One pathway by which Pacific ENSO SST variability can influence Africa is through the tropical troposphere (Fig. 1a). As an El Niño develops in July–August–September (JAS), positive SST anomalies promote anomalous ascending motion (deep convection) in the central and eastern equatorial Pacific, transporting heat to the troposphere. This anomalous deep convection drives a Gill–Matsuno response, triggering damped Kelvin and Rossby waves, which extend to the east and west of the heated region, respectively. The associated atmospheric Kelvin waves distribute the Pacific tropospheric heat throughout the tropics[18–20] (Fig. 1a). These warm tropospheric temperature anomalies enhance atmospheric stability outside the Pacific, in turn, suppressing atmospheric convection over West Africa and the Sahel[18], and decreasing rainfall[18,20]. This process also operates in other seasons.

The westward-propagating Rossby waves also initiated by the Gill–Matsuno response are similarly important. These Rossby waves establish high-pressure anomalies over the tropical Atlantic, the easterly wind anomalies of which weaken moisture transport from the Atlantic Ocean into West Africa, reducing the oceanic source of moisture for the Sahel, and thereby decreasing rainfall over the Sahel[21]. At the 100–200-mb level, the Rossby waves also weaken the Tropical Eastern African Jet, reducing upper-level divergence over regions of the Horn of Africa[22,23] and reducing rainfall.

The Indian Ocean

Also important in influencing ENSO impacts on the African climate are atmospheric teleconnection-driven interactions between Pacific Ocean SSTs and Indian Ocean SSTs. These connections involve interactions with modes of Indian Ocean SST variability (including the IOD, the IOB or the Subtropical Indian Ocean Dipole, in different seasons) or they can occur independently. For example, in JAS when the IOD is first developing, the interactions include a process that reinforces the troposphere warming mechanism. Specifically, as a result of El Niño in JAS, the western Pacific-minus-Indian Ocean zonal SST gradient weakens because of anomalous cooling in the west Pacific. The associated anomalous easterlies in the equatorial Indian Ocean push surface warm water to the central and western equatorial Indian Ocean, intensifying convection in that location[1,24,25]. Resulting anomalous upper-level easterlies in the western Indian Ocean, in combination with anomalous upper-level westerlies via the Atlantic (from enhanced convection in the central and eastern Pacific), form upper-level convergence. This convergence is conducive to large-scale subsidence over western Africa[21,24,25], driving negative rainfall anomalies.

In other seasons, the interactions with modes of Indian Ocean SST variability dominate. During September–October–November (SON), for example, El Niño influences the African climate in conjunction with the IOD (Fig. 1b). At this time, mature positive IOD (pIOD) phases — established through Bjerknes feedbacks — are common. ENSO processes act to reinforce this pIOD: El Niño-related weakening of the Walker circulation promotes easterly equatorial wind anomalies over the equatorial Indian Ocean, producing negative SST anomalies near Sumatra–Java and positive SST anomalies in the western Indian Ocean[1,26–28], an SST pattern resembling the pIOD (Fig. 1b). These SST anomalies cause a northwestward shift of atmospheric convection, a westward extension of the seasonal southeasterly trades[1,26,27], and an anomalously strong Intertropical Convergence Zone (ITCZ) over the

Box 1 | African seasonal circulation

The African climate varies by region and season. In mid-May, monsoonal rain reaches west Africa 5°N[18], and the cross-equatorial branch of the Somali Jet starts to bring moisture and rainfall northward to the southern slopes of the Ethiopian plateau. Toward June, the Saharan Heat Low establishes, the cyclonic circulation of which (aided by the development of the equatorial Atlantic cold tongue) connects southwesterly monsoonal flows and the northeasterly Mediterranean flows throughout the boreal summer months (June, July and August; JJA). These flows extend the Intertropical Convergence Zone (ITCZ) to ~17°N, and the tropical rain belt to around 10°N[18,31], explaining why 80% of the rain in the Sahel regions falls during these months[172].

During September, October and November, the tropical rain belt shifts southward, and Sahel rainfall dissipates. From October to early December, the onset of onshore moisture transport from the Indian Ocean drives coastal and topographic uplifts in the western highlands, producing short rains[5,173] across east African countries.

By austral summer (December–February; DJF), northeast trade winds blow across the northwest Indian Ocean, strong westerlies prevail over the equatorial Indian Ocean[5], and the subtropical Indian and Atlantic high-pressure systems are at their southernmost latitudes. These conditions lead to convergence over southern Africa, resulting in strong rainfall during these months. The convergence, uplift and instability, together with the upper-level divergence of the leading edge of midlatitude westerly troughs, support development of tropical–extratropical cloud-band events[12] (Tropical Temperate Troughs) that extend southeastward across southern Africa from the Angola Low toward the southwest Indian Ocean[9,13,172]. Also extending southeastward is the South Indian Convergence Zone (SICZ; blue dashed line in the upper right panel of the figure), which develops in southern summer and merges with the ITCZ over the southwest Indian Ocean[10]. The mid-level Botswana High, which forms in September–November in response to heat released by rainfall over the Congo Basin, shifts southward and strengthens into its peak in DJF[32].

During March, April and May, the ITCZ moves into the equatorial and southern equatorial Africa region. Onshore moisture transport from the Indian Ocean leads to high rainfall (the long rains)[5,16] across much of east Africa.

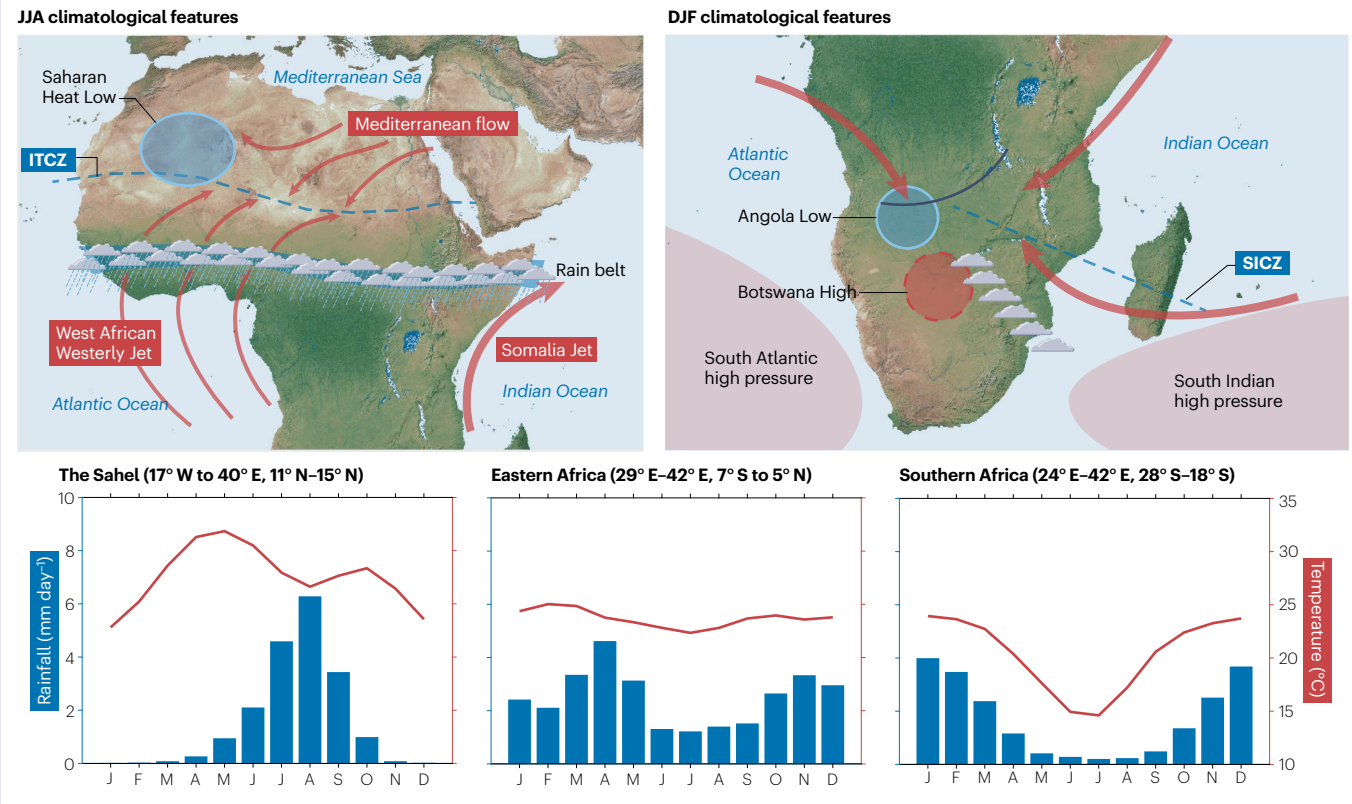

western Indian Ocean[26], increasing rainfall over north equatorial Indian Ocean and equatorial East Africa. Thus, part of ENSO's impact during SON is conveyed via the IOD, which by itself also exerts a similar impact to that of ENSO (cf. middle and right panels, Supplementary Fig. 1a).

In December–January–February (DJF), El Niño affects Africa through the IOB mode (Fig. 1c). In this season, the climatological winds along the equatorial Indian Ocean are westerlies, and no upwelling occurs in the equatorial eastern Indian Ocean. As in SON, El Niño-related

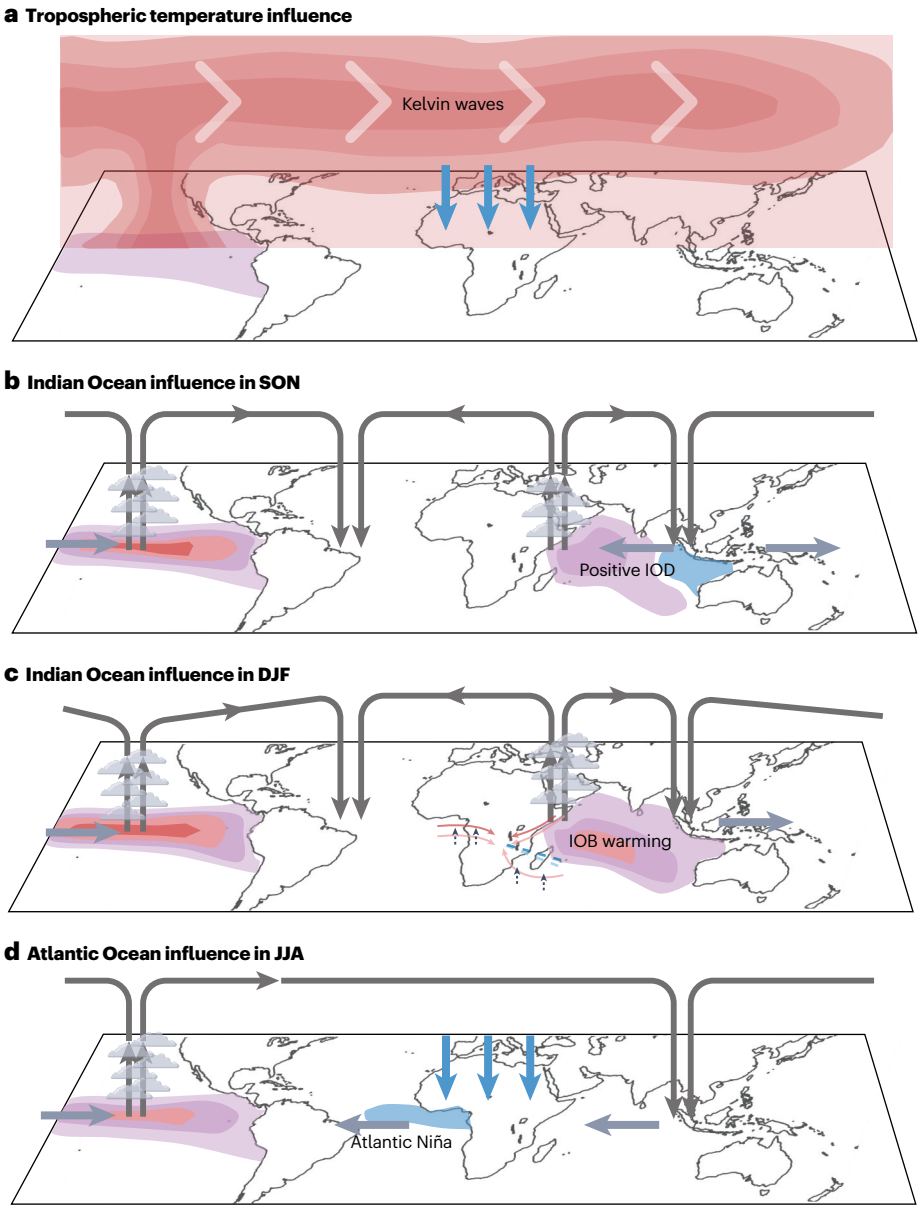

Fig. 1 | Mechanisms of impact of the El Niño–Southern Oscillation (ENSO) on African climate. a, Schematic representation of the tropospheric temperature mechanism, whereby El Niño triggers a Gill–Matsuno response, the atmospheric Kelvin waves (eastward arrows) of which increase atmospheric stability outside the Pacific, suppressing atmospheric convection (and thereby reducing rainfall) over the Sahel (blue downward arrows). **b**, Schematic representation of the Indian Ocean influence in September–October–November (SON), wherein El Niño weakens the Walker circulation (grey arrows), leading to a positive Indian Ocean Dipole (IOD) that enhances short rains in East Africa through increasing convergence toward East Africa. **c**, As in panel **b**, but during December–January–February (DJF) when El Niño-related Walker circulation weakening causes Indian Ocean Basin mode (IOB) warming that reduces the land–ocean pressure gradient, and lowers the southward extension of seasonal flow convergence and the equatorward shift of the South Indian Convergence Zone equatorward compared with the climatology (light versus dark arrows), in turn, increasing rainfall in northeast southern Africa but decreasing it in southeast southern Africa. **d**, Schematic representation of the Atlantic Ocean influence in June–July–August (JJA), whereby El Niño-related weakening of the Walker circulation drives development of an Atlantic Niña that shifts the tropical rain belt northward, decreasing rainfall over the Guinea coast but increasing rainfall over the Sahel; this increased Sahel rainfall competes with rainfall reductions via the tropospheric temperature mechanism in panel **a**. Thus, El Niño influences African climate through troposphere temperature warming and concurrent modes of variability in the Indian Ocean and the Atlantic oceans.

weakening of the Walker circulation establishes easterly wind anomalies in the equatorial Indian Ocean. These wind anomalies reduce the prevailing westerlies, subsequently decreasing evaporative heat loss and generating basin-wide warm anomalies[3]; this warming is also reinforced by the tropospheric temperature warming process. Basin-wide warming, in turn, strengthens convection over the tropical Indian

Ocean and weakens the pressure gradient between the ocean and the African continent[5,29,30]. A resulting decrease in seasonal converging flows induces circulation changes over much of southern Africa, including weaker southward excursion of the South Indian Convergence Zone (SICZ)[10,31], an intensified mid-level Botswana High[32], a weakened Angola Low[33] and a shallowed Mozambique Channel Trough[34] (Fig. 1c). Through these processes, rainfall can be perturbed across much of southern Africa. The influence of the IOB warming persists into March–April–May (MAM), with some conditions unfavourable for moisture transport into southern Africa continuing.

In addition, El Niño impacts on DJF Africa rainfall are conducted through a negative phase of the Subtropical Indian Ocean Dipole[35–37]. During a negative phase, cold SST anomalies south of Madagascar decrease moisture transport into southeastern Africa, favouring anomalously dry and hot summers. In contrast, warm SST anomalies to the north cause anomalously wet and cold conditions over eastern Africa[35] (Supplementary Fig. 1b). However, this impact is not statistically significant after ENSO influence is removed (cf. centre and right panels, Supplementary Fig. 1b), highlighting that the Subtropical Indian Ocean Dipole is, by and large, a response of the subtropical highs to ENSO.

The processes described above for El Niño apply in the opposite sense to La Niña. As a La Niña develops, the troposphere cools throughout the tropics, conducive to the ascending motion and rainfall over the Sahel region. Convection over the western equatorial Pacific intensifies, creating an anomalously strong Walker circulation with anomalous westerlies over the Indian Ocean[2,16], often coinciding with a negative IOD in JJA and SON. These changes strengthen the upper-level easterlies, leading to increased subsidence and decreased rainfall over eastern Africa. The anomalous westerlies drive an IOB cooling, delivering opposite impacts to those of El Niño.

The Atlantic Ocean

The Atlantic Ocean also has a role in modulating ENSO impacts on the African climate, largely through co-occurrence with an Atlantic Niño or Atlantic Niña. Through the weakened Walker circulation, an El Niño induces easterly anomalies along the equatorial Atlantic, the resulting upwelling of which drives cool SST anomalies in the east, in turn promoting dry anomalies over the Guinea coast and wet anomalies over the Sahel[6,31]. This dipole rainfall pattern is similar to that associated with Atlantic Niña (Supplementary Fig. 1c): decreased rainfall over the Guinea coast and increased rainfall in the Sahel, both linked to easterly wind anomalies, increased upwelling, cooled SSTs, suppressed atmospheric convection, northward-shifted tropical rain belt and ITCZ, intensified land–ocean thermal and pressure gradients, and strengthened northward monsoon penetration into West Africa[4,38–41]. Thus, co-occurrence of an Atlantic Niña and El Niño — as is often the case — amplifies the dipolar rainfall pattern (Fig. 1d). However, wet anomalies in the Sahel can be offset by the increased subsidence arising from the tropospheric temperature mechanism[4,19,38,40]. Indeed, should that occur, the concurrent Atlantic Niña broadens the El Niño-induced drying from Senegal to Ethiopia[42].

Modulations of ENSO impact on Africa

Beyond SSTs in the Indian and Atlantic Ocean, ENSO's impact on the African climate is also modulated by various other processes and features. These include Mediterranean SST, the Southern Annular Mode (SAM), and regional circulations (encompassing the Sahara Heat Low, the Somali Jet, the Angola Low, the Boswana High and the SICZ), as now discussed. Note that although these circulation systems can respond to ENSO, they also vary independently to modulate ENSO impact.

Mediterranean SSTs. Mediterranean SST can substantially affect the West African monsoon and modulate ENSO impact. Warmer-than-normal Mediterranean SSTs enhance local evaporation, increasing northward moisture advection and continental moisture flux convergence in low-level northern Africa[43]. As a result, the West African monsoon is intensified and the tropical rainband (see Box 1 figure) migrates northward[43,44], increasing Sahel rainfall. The amplitude of the Sahel rainfall anomalies is comparable with those from ENSO. Moreover, anomalously high SSTs in the eastern Mediterranean relative to the Indian Ocean are conducive to increased rainfall over the Sudan–Sahel region; this enhancement occurs via strengthened low-level convergence between the northeasterly moisture transport from the eastern Mediterranean and the monsoonal southwesterly moisture transport from the eastern equatorial Atlantic[44]. Thus, variability in Mediterranean SSTs can modify ENSO impact: an El Niño concurrent with warmer-than-normal Mediterranean SSTs is associated with subdued rainfall in West African, Sahel and Sudan–Sahel regions, but El Niño concurrent with cooler-than-normal Mediterranean SSTs is associated with amplified dry conditions.

The Southern Annular Mode. Modes of high-latitude climate variability can also exert a control on ENSO–rainfall relationships in Africa, including the SAM. During a negative phase of the SAM, the midlatitude westerlies are shifted equatorward, bringing frontal systems[45] and low-level moisture fluxes toward southern Africa, increasing rainfall in western South Africa during JJA[46]. However, in DJF, the associated easterly flows from the Indian Ocean to eastern South Africa decrease[47], reducing rainfall. An equatorward shift of the atmosphere circulation during El Niño in DJF tends to induce a negative phase of the SAM, thereby reinforcing El Niño-induced dry conditions over South Africa in DJF. Thus, an El Niño concurrent with a negative SAM phase, amplifies JJA rainfall increases in western South Africa and DJF drying over eastern South Africa.

Regional circulations. ENSO impacts on the African climate are also modulated by regional circulations that vary both independently and respond to ENSO. The Saharan Heat Low — a low-pressure system situated over the Sahara in the summer months whose intensity varies on intraseasonal to interdecadal timescales[48,49] — is one such example. In combination with the relative high pressure over the Guinean coast, the Sahara Low produces a low-level pressure gradient that drives the West African monsoon: the stronger the Sahara Low, the more intense the monsoonal flow[48]. In addition, an intensified Saharan Heat Low favours a mid-level African Easterly Jet[50], with corresponding divergence driving convection over the Central and Eastern Sahel, but decreased convection from Senegal to west of the Jos Plateau[49]. Thus, variability of the heat low modifies ENSO impact: when an El Niño occurs with an anomalously strong heat low, the impact of El Niño can be muted.

Likewise, the Somali Jet — which develops during April–June and brings moisture to the southern slopes of the Ethiopian plateau and the Greater Horn of Africa[51,52] — has a bearing on ENSO impact. Typically, a stronger jet is associated with anomalously high rainfall in these regions, and vice versa[53,54]. During El Niño, however, there is a tendency for delayed onset and reduced intensity of the Somali Jet; thus, many drought years over the Ethiopian plateau coincide with an El Niño[8,54]. However, the Somali Jet can be influenced by other factors (including cross-equatorial and land–sea temperature gradients) such

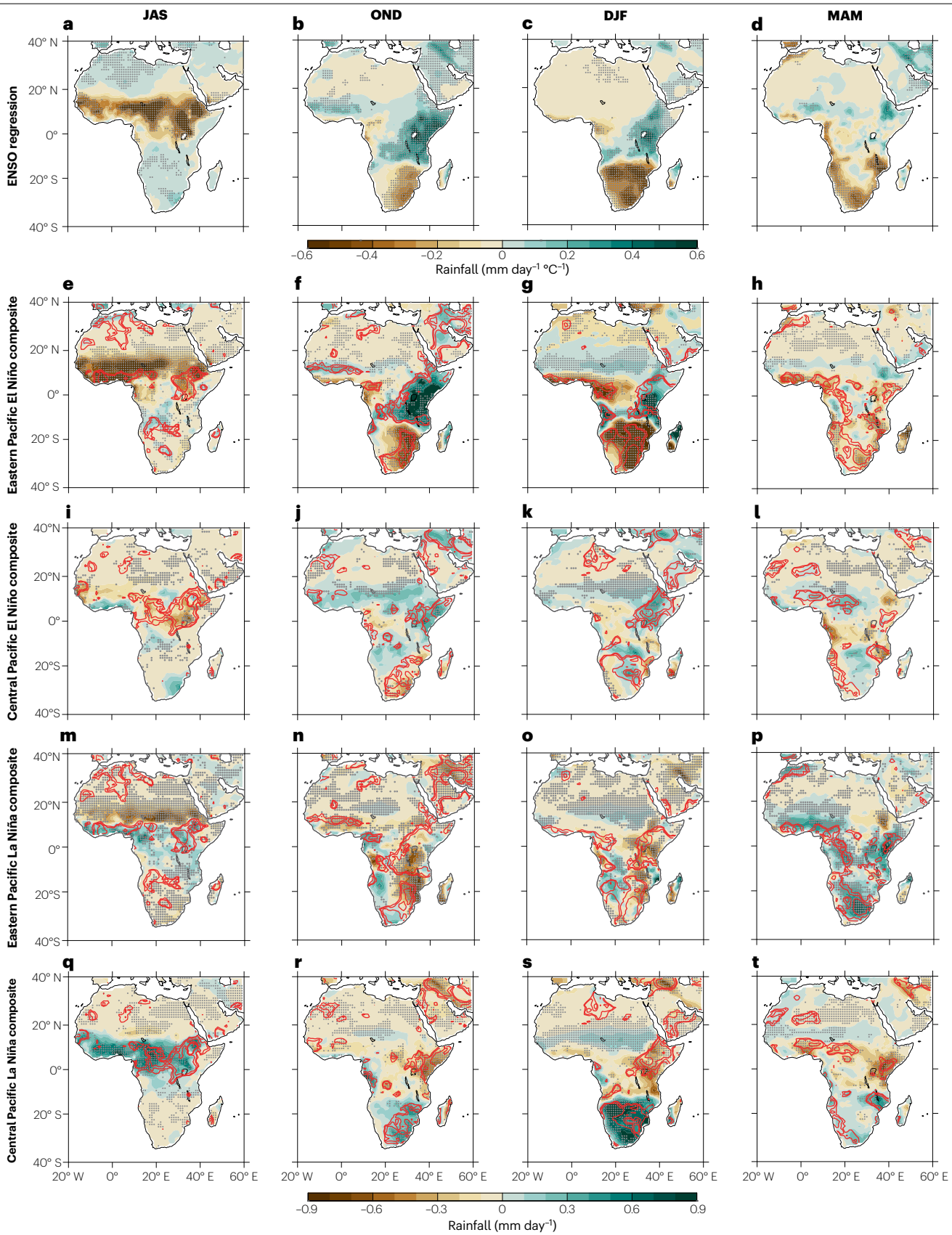
JAS
OND
DJF
MAM
a
b
c
d
ENSO regression
40° N
20° N
0°
20° S
40° S
−0.6
−0.4
−0.2
0
0.2
0.4
0.6
Rainfall (mm day⁻¹ °C⁻¹)
e
f
g
h
Eastern Pacific El Niño composite
i
j
k
l
Central Pacific El Niño composite
m
n
o
p
Eastern Pacific La Niña composite
q
r
s
t
Central Pacific La Niña composite
20° W
0°
20° E
40° E
60° E
−0.9
−0.6
−0.3
0
0.3
0.6
0.9
Rainfall (mm day⁻¹)

Fig. 2 | Seasonal evolution of observed ENSO impacts on African rainfall. **a**, July–August–September (JAS) rainfall anomalies averaged across four datasets[162–164] regressed onto a normalized Niño3.4 index averaged across three datasets[165–167] at zero lag over 1948–2023; stippling indicates statistical significance above the 95% confidence level. **b**–**d**, As in panel **a**, but for October–November–December (OND), December–January–February (DJF) and March–April–May (MAM). **e**, Composites of JAS rainfall anomalies averaged across four datasets[162–164,168] during eastern Pacific El Niño events over 1948–2024 wherein the E-index[66] is >1 standard deviation. Stippling indicates consistency in the sign of anomalies for 70% of El Niño–Southern Oscillation (ENSO) events, and red contours mark anomalies significant at the 90%, 95% and 99% confidence levels. **e**–**h**, As in panel **d**, but for OND, DJF and MAM. **i**–**l**, As in **a**–**d**, but for central Pacific El Niño events wherein the C-index[66] is >1 standard deviation. **m**–**p**, As in **a**–**d**, but for eastern Pacific La Niña events wherein the E-index is <−1 standard deviations. **q**–**t**, As in **i**–**l** but for central Pacific La Niña events where the C-index is <−1 standard deviations. ENSO affects different regions in different seasons through different mechanisms, with generally opposite but asymmetric impacts between El Niño and La Niña.

that the standard ENSO–Somali Jet relationship can differ and thereby modulate ENSO impact; thus not all El Niño events lead to a drought over the plateau.

The Angola Low is an additional factor influencing the impact of ENSO in Africa. The Angola Low represents the climatological aggregate of summertime tropical lows that form following the breakdown of the Congo Air Boundary[9,55]. Typically, an anomalously weak or northward Angola Low promotes increased rainfall over tropical southern Africa but decreased rainfall over subtropical southern Africa[55]; the reverse prevails for an anomalously strong or southward Angola Low. The position and intensity of the Angola Low is influenced by ENSO, weakening and shifting northward during El Niño and intensifying and shifting southward during La Niña[9], thereby modulating any rainfall responses[56]. However, the response of the Angola Low can be vastly different from one event to another. For example, the Angola Low barely weakened during the 1997/98 El Niño, meaning that an expected drought did not eventuate over southern Africa[30].

Like the Angola Low, variability in the Botswana High also has a role. Situated across tropical southern Africa, the Botswana High typically forms in August, and strengthens and moves southward during austral spring and summer[32,57,58]. Its strength varies independently and dependently of ENSO[57]. During El Niño summers, the Botswana High tends to intensify[57,58], reducing moisture transport from the tropical Indian Ocean and establishing extremely dry conditions across most of southern Africa, as during the 2015/16 El Niño event[30]. Yet the magnitude of Botswana High anomalies is not proportional to the strength of ENSO events. For example, during the 1997/98 strong El Niño event the high was less intense than in the weaker 1986/1987 El Niño event[30,58], contributing to variability in hydroclimatic responses.

Similarly, the Tropical Temperate Trough is an important determinant of ENSO–rainfall connections in Africa. The Tropical Temperate Trough is a cloud-band system of convergence and convection extending northwest–southeast over southern Africa to the southwest Indian Ocean, inducing heavy rainfall[13,33,59,60]. During El Niño, convergence shifts northward and troughs tend to be less common[9,55], whereas during La Niña, troughs form more frequently and shift further south[9,33,55,61]. Yet the Tropical Temperate Trough also varies independently of ENSO, as seen during the 1997/98 El Niño (when troughs are typically uncommon), which witnessed a quick succession of two trough events that contributed >40% of summer rainfall over much of southern Africa[62].

Finally, African rainfall is also influenced by the SICZ, a large-scale summer land-based convergence zone that extends across southern Africa into the southwest Indian Ocean[10,63]. A northward shift of the SICZ reduces moisture transport from the Indian Ocean[64], leading to increased rainfall in the northeast and decreased rainfall in the southwest. During El Niño, the SICZ shifts northeastward, owing to a weakening in the western portion of the South Indian High[10]. Accordingly, rainfall increases in the northeast and decreases in the southwest.

Thus, ENSO impact on the African climate involves various mechanisms. These mechanisms include tropical tropospheric planetary-wave propagation, interbasin interactions with the Indian and Atlantic oceans, and extratropical processes. The impacts are also modulated by regional circulations.

ENSO effects on the African climate

Having established the physical mechanisms by which ENSO can influence the African climate, attention is now turned to their corresponding impacts. The seasonal evolution of ENSO–rainfall relationships is discussed (Fig. 2), outlining first the symmetric assumptions (the linearly opposite El Niño and La Niña responses captured through regression analysis) and second their asymmetric components (the contrasting impacts captured by composite analysis). The latter can be substantial, owing to ENSO asymmetries related to: the SST anomaly centre (eastern Pacific (EP ENSO) or central Pacific (CP ENSO)[65–68]); the magnitude of SST anomalies (EP El Niño is greater than CP El Niño[65–67,69,70], CP La Niña tends to be greater than EP La Niña[65,66,71–73], and strong El Niño tends to be greater than strong La Niña[52,54,56]); and the duration of events (La Niña tends to last multiple years but that is rare for El Niño). Composites based on EP and CP ENSO indices, constructed as a linear combination of the first two empirical orthogonal functions of DJF SST anomalies in the tropical Pacific[66,68–70] (Supplementary Fig. 3a,b), allow these asymmetries to be determined.

JAS

In JAS, ENSO–African relationships are dominated by anomalies in the Sahel and surrounding regions. Here, strong warming and drying occur during the El Niño developing months[6,31,39] (Fig. 2a; Supplementary Fig. 2a), with Sahel-averaged anomalies (11–15° N, 17° W to 40° E) reaching 0.38 °C °C^{-1} and −0.42 mm day^{-1} °C^{-1}. Remnant SST anomalies from the 1982/83 strong El Niño, for example, led to the 1983 boreal summer drought over the western Sahel[74], one of the driest summers of the twentieth century for the region. These impacts can largely be linked to the tropical troposphere temperature mechanism (Fig. 1a) which increases atmospheric stability, suppresses convection, and weakens circulation and moisture transport over the Sahel[18,20]. Upper-level convergence associated with anomalous winds from the Atlantic and Indian Oceans also contributes to subsidence over western Africa, decreasing the frequency of wet days and heavy rainfall events across the Guinea coast and into the Sahel during early-peak West African monsoon season[21,24,25].

By definition, the opposite JAS effects would be observed in the Sahel during La Niña developing years if one assumes that ENSO is a linear system (opposite-signed anomalies of Fig. 2a, Supplementary Fig. 2a). For example, during the 1998 La Niña, rainfall over the Sahel was anomalously high[39]. These relationships would emerge from tropospheric cooling that promotes atmosphere instability over the Sahel,

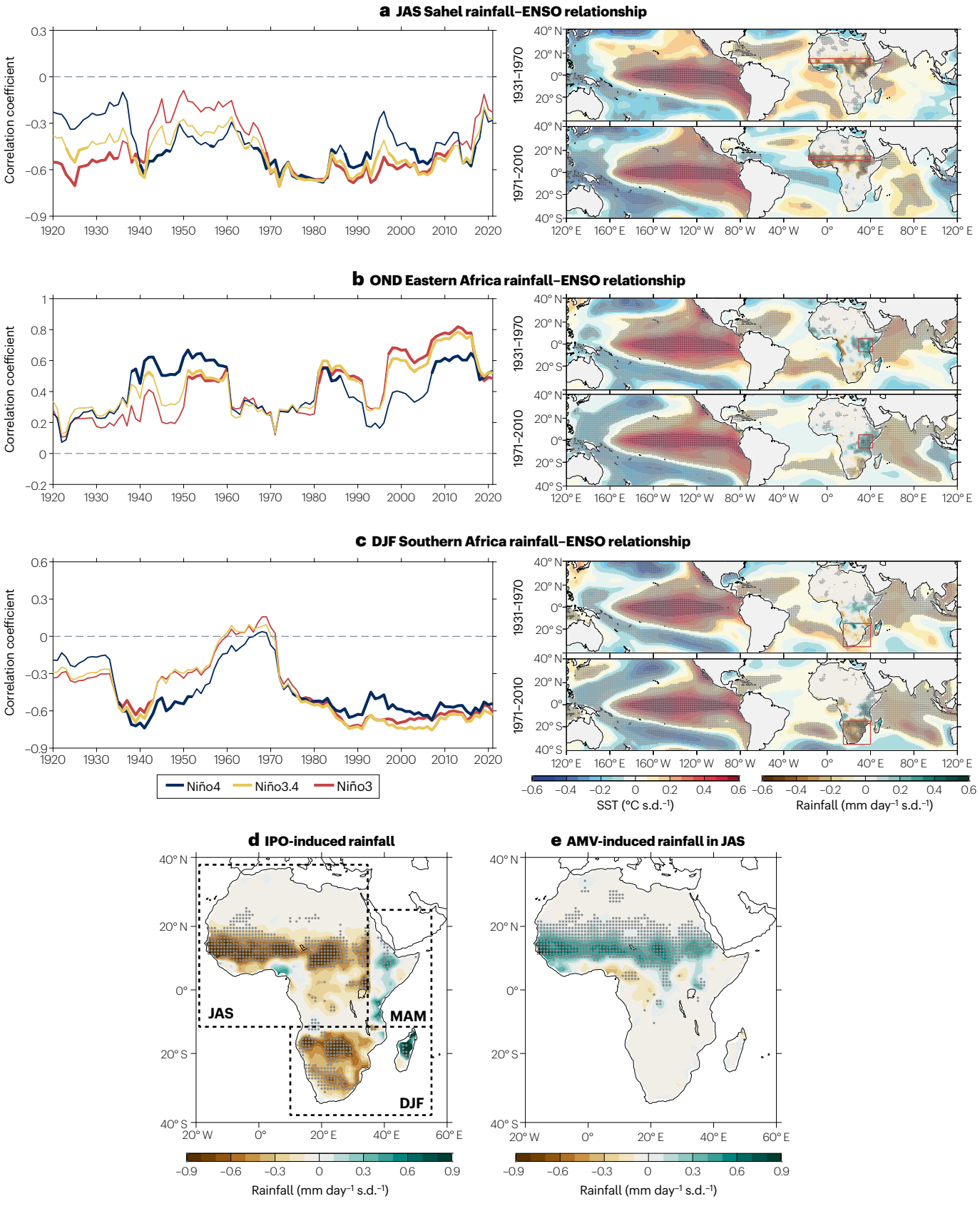
a JAS Sahel rainfall–ENSO relationship
Correlation coefficient
0.3
0
−0.3
−0.6
−0.9
1920 1930 1940 1950 1960 1970 1980 1990 2000 2010 2020
1931–1970
1971–2010
40° N
20° N
0°
20° S
40° S
120° E 160° E 160° W 120° W 80° W 40° W 0° 40° E 80° E 120° E
b OND Eastern Africa rainfall–ENSO relationship
Correlation coefficient
1
0.8
0.6
0.4
0.2
0
−0.2
1920 1930 1940 1950 1960 1970 1980 1990 2000 2010 2020
1931–1970
1971–2010
c DJF Southern Africa rainfall–ENSO relationship
Correlation coefficient
0.6
0.3
0
−0.3
−0.6
−0.9
1920 1930 1940 1950 1960 1970 1980 1990 2000 2010 2020
Niño4
Niño3.4
Niño3
1931–1970
1971–2010
120° E 160° E 160° W 120° W 80° W 40° W 0° 40° E 80° E 120° E
−0.6 −0.4 −0.2 0 0.2 0.4 0.6
SST (°C s.d.⁻¹)
−0.6 −0.4 −0.2 0 0.2 0.4 0.6
Rainfall (mm day⁻¹ s.d.⁻¹)
d IPO-induced rainfall
40° N
20° N
0°
20° S
40° S
JAS
MAM
DJF
20° W 0° 20° E 40° E 60° E
−0.9 −0.6 −0.3 0 0.3 0.6 0.9
Rainfall (mm day⁻¹ s.d.⁻¹)
e AMV-induced rainfall in JAS
40° N
20° N
0°
20° S
40° S
20° W 0° 20° E 40° E 60° E
−0.9 −0.6 −0.3 0 0.3 0.6 0.9
Rainfall (mm day⁻¹ s.d.⁻¹)

Fig. 3 | Influence of decadal variability on ENSO–rainfall relationships in Africa. a, Relationships between Sahel rainfall and the El Niño–Southern Oscillation (ENSO) during July–August–September (JAS), including: observed 20-year running correlation between 11-year high-pass filtered JAS Sahel rainfall anomalies[168] (17° W to 40° E,11–15° N; red box in the right panels) and 11-year high-pass filtered JAS ENSO indices, with thicker lines indicating correlations significant above the 95% confidence level (left); and regression of sea surface temperature[169] and rainfall[168] anomalies onto normalized Niño3.4 index averaged across three datasets[165–167] over 1931–1970 (top right) and 1971–2010 (bottom right). **b**, As in panel **a**, but eastern Africa rainfall–ENSO relationships during October–November–December (OND), with eastern Africa encompassing 29–42° E, 7° S to 5° N. **c**, As in panel **a**, but southern Africa rainfall–ENSO relationships during December–January–February (DJF), with southern Africa encompassing 15–40° E, 15–35° S. **d**, Regression of seasonal rainfall anomalies[168] in different parts of Africa onto a normalized 11-year low-pass filtered annual mean Interdecadal Pacific Oscillation (IPO) time series[170] over 1901–2022; western and northern Africa (20° W to 35° E, 12° S to 40° N) focus on JAS, eastern Africa (35–55° E, 12° S to 25° N) on MAM, and southern Africa (10–55° E, 12–38° S) on DJF. **e**, Regression of JAS rainfall anomalies[168] onto normalized 11-year low-pass filtered annual mean Atlantic Multidecadal Variability (AMV) time series[171] over 1901–2022. In all panels, stippling indicates statistical significance above the 95% confidence level. Decadal variability modulates ENSO impact but also induces decadal anomalies on which ENSO anomalies are superimposed.

and upper-level divergence that promotes large-scale ascent over western Africa, both conducive to increased rainfall[21].

In reality, however, ENSO nonlinearity translates into nonlinear climate impacts over the Sahel. For instance, negative El Niño-related precipitation anomalies are much stronger for EP events (−0.73 mm day^{-1}; Fig. 2e) relative to CP events (−0.12 mm day^{-1}; Fig. 2i). For example, the 1997 EP El Niño and the 2009 CP El Niño produced average Sahel rainfall anomalies of −80.0 and −10.0 mm day^{-1}, respectively. These differences arise from the larger amplitude of EP El Niño SST anomalies compared with the CP El Niño, triggering a stronger tropospheric temperature response. In addition, strong SST cooling in the equatorial eastern Atlantic coherent with EP El Niño[75], but weaker in CP El Niño, suppresses atmospheric convection and contributes to rainfall reductions. By contrast, CP La Niña events tend to be much stronger than EP La Niña in amplitude[71,72], as reflected in the magnitude of corresponding rainfall anomalies over Africa. Indeed, positive La Niña-induced rainfall anomalies over the Sahel are larger for CP events (+0.30 mm day^{-1}; Fig. 2q) than for EP events (+0.12 mm day^{-1}; Fig. 2m).

OND

As the ENSO cycle develops into OND, the spatial pattern of climate impacts evolves to include dipole centres of action between eastern (and central) Africa and southern Africa. During El Niño, anomalously high rainfall occurs during the short rain season in East Africa[1,26–28] (Fig. 2b), with spatially averaged changes of +0.38 mm day^{-1} °C^{-1} (7° S to 5° N, 29–42° E). For example, during the 1997 El Niño event, devastating floods in Somalia, Ethiopia, Kenya, Sudan and Uganda caused several thousand deaths and displaced hundreds of thousands of people[1]. These changes can be linked to a weakened Walker circulation, the anomalous equatorial easterlies associated with a concurrent pIOD event (Fig. 1b) and the anomalously strong ITCZ over the western Indian Ocean[26], collectively promoting low-level warm moist convergence toward the equatorial east coast of Africa. Surface air temperature anomalies are small, owing to an offset between increases from western ocean warming and decreases from enhanced evaporation (Supplementary Fig. 2b).

The other centre of action in OND is statistically significant warming and drying in South Africa. Here, anomalies reach 0.14 °C °C^{-1} and −0.15 mm day^{-1} °C^{-1} over 35–15° S, 15–40° E (Fig. 2b; Supplementary Fig. 2b). Indeed, during 2015 El Niño, the anomalies were 0.97 °C °C^{-1} and −0.67 mm day^{-1} °C^{-1}. These dry and warm anomalies develop as the seasonal southward excursion of the SICZ and cloud-band events are impeded and shift northeastward to the off-equatorial regions[5,10,33,62].

There is strong evidence of the opposite effects during La Niña. Indeed, the three consecutive La Niña from 2020 to 2022 led to failed rain seasons across Kenya, Somalia and Ethiopia, causing food shortage and acute malnutrition[17]. By contrast, rainfall increased over south Africa, averaging 0.20 mm day^{-1} over the three summers. These impacts arise from a strengthened Walker circulation and resulting anomalous westerlies over the equatorial Indian Ocean that shift low-level convergence to the eastern Indian Ocean/western Pacific region, causing drier-than-normal conditions. Likewise, over southern Africa, the SICZ and cloud-band events extended further south.

As in DJF, there is substantial nonlinearity to these responses. Once again, the stronger-amplitude SST anomalies for EP El Niño relative to CP El Niño translate into a stronger and more coherent rainfall dipole[76]: +0.90 mm day^{-1} over east Africa and −0.33 mm day^{-1} over southern Africa for EP (Fig. 2f), versus +0.22 mm day^{-1} and −0.09 mm day^{-1} for CP (Fig. 2j). The differences are reflected in individual events: +0.25 mm day^{-1} and −0.14 mm day^{-1} during the 2009 CP El Niño, but +0.92 mm day^{-1} and −0.67 mm day^{-1} during the 2015 strong El Niño. Similarly, the weaker SST anomalies for EP La Niña compared with CP La Niña give rise to a weaker and less spatially coherent precipitation dipole for the former: −0.22 mm day^{-1} over East Africa and 0.06 mm day^{-1} over southern Africa for EP La Niña (Fig. 2n), versus −0.27 mm day^{-1} and 0.22 mm day^{-1} for CP La Niña (Fig. 2r). This asymmetry between EP El Niño (+0.90 mm day^{-1}) and CP La Niña (−0.27 mm day^{-1}) rainfall anomalies is, in part, related to the stronger El Niño-induced pIOD compared with the La Niña-induced nIOD[70].

DJF

The spatial pattern of ENSO-related anomalies in DJF is broadly similar to OND, consisting of opposite responses between southern Africa and eastern Africa. For El Niño, warmer and drier conditions dominate across southern Africa[5,30] (Fig. 2c; Supplementary Fig. 2c), averaging 0.28 °C °C^{-1} and −0.37 mm day^{-1} °C^{-1} when averaged over 35–15° S, 15–40° E. Prolonged dry spells during the 2023/24 El Niño, for example, resulted in widespread crop failure and livestock losses, according to the World Food Programme[77]. This reduction in precipitation is linked to subsidence-related suppression of low-level southward moisture convergence and cloud-band development[33]. The subsidence is related to convection strengthening over the tropical Indian Ocean and pressure gradient weakening between the ocean and the African continent as a result of IOB warming (Fig. 1c). The decrease in rainfall leads to an increase in solar radiation and evaporation, in turn increasing surface temperature by 0.45 °C.

The other node of the dipole encompasses wet anomalies across East Africa. Here, rainfall increases of +0.29 mm day^{-1} °C^{-1} are associated with El Niño (Fig. 2c; Supplementary Fig. 2c). This above-average rainfall occurs because the seasonal southward excursion of the

SICZ and cloud-band events are impeded and shift northeastward to the off-equatorial regions[10,33] (Fig. 1c). Like in OND, surface air temperature anomalies are small because increases due to the western ocean warming are offset by decreases from enhanced evaporation (Supplementary Fig. 2c).

The opposite impacts occur during La Niña. Specifically, decreased rainfall is observed over the equatorial East African regions and increased rainfall over south Africa. These impacts arise from a strengthened Walker circulation, leading to a shift low-level convergence to the eastern Indian Ocean, causing the drier-than-normal conditions over equatorial Africa, but the SICZ and cloud-band events extend further south, increasing rainfall and decreasing air temperatures over southern Africa.

Nonlinearities in these responses are particularly marked during DJF. For instance, whereas a strong dipole is apparent between eastern and southern Africa for EP El Niño (+0.72 mm day^{-1} and −0.70 mm day^{-1}, respectively; Fig. 3g), it is far weaker and less defined for CP El Niño[76] (+0.04 mm day^{-1} and −0.003 mm day^{-1}; Fig. 3k). Moreover, for EP El Niño events there is strong subsidence-related drying toward the Guinea coast[31,40] that is absent for CP El Niño (Fig. 3g,k). Likewise, the eastern and southern Africa precipitation anomaly is ill defined and weak for EP La Niña (−0.04 mm day^{-1} and −0.32 mm day^{-1}, respectively; Fig. 3o) compared with CP La Niña[76] (+0.64 mm day^{-1} and −0.33 mm day^{-1}; Fig. 3s). These differences primarily reflect the weaker SST anomalies of EP La Niña compared with CP La Niña.

MAM

In MAM after an El Niño, the impacts on Africa largely reflect drying over southern Africa with little wet anomaly in off-equatorial East Africa. Specifically, although more geographically constrained, warm and dry conditions persist from DJF[5,30] (Fig. 2d; Supplementary Fig. 2d), averaging 0.44 °C °C^{-1} and −0.19 mm day^{-1} °C^{-1}, respectively. The warm and dry anomalies emerge from continued El Niño-induced IOB warming, strengthened convection over the tropical Indian Ocean, and a weakened pressure gradient between the ocean and the African continent, both of which increase subsidence over southern Africa.

In MAM after a La Niña, these impacts generally reverse. Wet conditions predominate over southern Africa, arising from a weakening in convection over the tropical Indian Ocean and an intensification in the pressure gradient between the ocean and the African continent — conditions that continue from DJF. These dynamics increase low-level moisture convergence, facilitating cloud-band development and rainfall over land[33].

As in other seasons, however, there is a substantial asymmetry in these teleconnections. For example, the dry anomaly over southern Africa is strong after an EP El Niño compared with CP El Niño (Fig. 2h,l). Further, dry anomalies over off-equatorial East Africa are generated during CP La Niña, but anomalies are far weaker during EP La Niña (Fig. 2p,t). El Niño events often transition into a developing La Niña[66,71]. The transition leads to a dry short rain season in eastern Africa[5,16]. During such transitions, when SST in the tropical western Pacific is high[16], moisture transport increases to the west, decreasing rainfall in the long rain season. Such a sequence occurred in 2016–2017, when the 2015/16 El Niño transitioned to a La Niña[16–18]. By contrast, a CP La Niña often persists into a multiyear La Niña event[71,78]. Accordingly, the associated eastward shift of convergence toward the Indo-Pacific region induces a dry anomaly (−0.38 mm day^{-1}) over East Africa (Fig. 2t), leading to a multiyear decrease in long rain. There is no counterpart for EP El Niño, as a strong El Niño event usually does not continue into the next year.

Multidecadal variability

In addition to ENSO variability, temporal fluctuations in ENSO–Africa impacts add to their complexity. These multidecadal changes are evident across many regions of Africa[6,24,79,80], particularly between 1931–1970 and 1971–2010, time periods of generally weakened and strengthened interbasin interactions, respectively. These multidecadal changes are now discussed for the Sahel, eastern Africa and Southern Africa (Fig. 3).

In the Sahel, ENSO's impact on rainfall varies markedly from 1931–70 and 1971–2010. Pre-1970s, correlations between ENSO (Niño3.4) and Sahel rainfall averaged −0.43 (Fig. 3a, left), and accordingly, El Niño-induced decreases in JAS Sahel rainfall were small at −0.29 mm day^{-1} (standard deviation (s.d.))$^{-1}$ (Fig. 3a, right); these relationships generally also hold for Niño3 and Niño4 indices. These comparatively low-amplitude anomalies relate to the relatively weak magnitude of El Niño events[81,82] (Fig. 3a, right), warm SSTs in the North Atlantic (relative to the tropics elsewhere)[83] and weak covariability between El Niño and Atlantic Niña[4,20,40]. In contrast, El Niño relationships with Sahel rainfall are much stronger during 1971–2010, with average correlations reaching −0.59 (Fig. 3a, left) and corresponding rainfall anomalies reaching −0.43 mm day^{-1} s.d.$^{-1}$ (Fig. 3a, right). This change in relationship can be linked to more coherency in modes of tropical SST variability between the three oceans[6,24,31,79,80,84]. Indeed, during 1971–2010, a negative phase of Atlantic Multidecadal Variability (AMV) enhanced covariability between ENSO and Atlantic Niña/Niño[6,20,85], decreasing occurrences of the Atlantic Niña/Niño-related rainfall dipole pattern[6,24,86] as Pacific-related anomalies dominate[87,88].

Similar decadal fluctuations in ENSO impact occur in East Africa. ENSO–rainfall relationships are again generally weaker during 1931–70 (r = 0.30) compared with 1970–2010 (r = 0.61), albeit with more decadal variability (Fig. 3b, left). Accordingly, OND El Niño-related rainfall anomalies averaged over East Africa vary from 0.29 mm day^{-1} s.d.$^{-1}$ in the early period to 0.34 mm day^{-1} s.d.$^{-1}$ in the later period (Fig. 3b, right). The stronger relationships during 1971–2010 can be linked to enhanced ENSO–IOD coupling[89], with strong equatorial Indian Ocean easterlies and a westward shift in the Indian Ocean ITCZ intensifying the short rain response to ENSO[90] and driving a strong wet anomaly over the Horn of Africa[2]. Since the turn of the twenty-first century, a decreased ENSO–IOD relationship[91] contributes to the observed reduction in the impact of El Niño on east Africa rainfall (Fig. 3a, left).

Summer rainfall over southern Africa also shows pronounced decadal variability. During 1931–70, correlations between ENSO and DJF rainfall are 0.15 and rainfall anomalies averaged over the region are −0.05 mm day^{-1} s.d.$^{-1}$, far lower than correlations of −0.69 and anomalies of −0.33 mm day^{-1} s.d.$^{-1}$ seen from 1971–2010 (Fig. 3c). This relationship intensification can also be explained by strengthened ENSO–IOD coupling during 1971–2010, leading to a reversal of the Walker circulation over the western tropical Indian Ocean[92] and a strong negative subtropical Indian Ocean Dipole[93] during DJF, both contributing to the low rainfall in southern Africa. Additionally, a positive phase of the Interdecadal Pacific Oscillation (IPO) during 1971–2010 is associated with more El Niño events and an overall stronger impact by the ENSO on southern Africa[94].

Any changes in ENSO relationships can be modulated by multidecadal SST fluctuations that influence climatological rainfall. For example, a positive IPO from the late 1960s to the late 1980s contributed to a widespread decrease in Sahel rainfall during JAS[95,96] (Fig. 3d). Rainfall reductions linked to the 1982/83 El Niño therefore contributed to a near-record Sahel drought[74]. A positive IPO is further

associated with reduced moisture convergence and vertical ascent over southern Africa (including the Limpopo River Basin), decreasing summertime cloud-band formation and rainfall[97,98], and thereby modulating any ENSO impacts in the region, for example El Niño-induced drought (Fig. 3d).

The transition into a negative phase of the IPO since the late 1990s is also important. The strengthened Walker circulation post-1990s associated with the negative IPO results in warming in the central and eastern Indian Ocean[99], reducing moisture transport to equatorial eastern Africa, leading to drying of the East African long rains[100–102] (Fig. 3d), increasing the susceptibility to long-rain drought during La Niña events, and heightening the risk of ENSO-induced consecutive short-rain and long-rain droughts[16]. Through the troposphere temperature mechanism, the negative IPO has also contributed to Sahel rainfall recovery, increasing extreme rainfall events during La Niña years[103].

The phase of the AMV likewise has a bearing on ENSO-related rainfall anomalies in Africa. A negative phase of the AMV (reflecting lower SSTs in the tropical North Atlantic and Mediterranean Sea relative to the tropical South Atlantic) decreases meridional moisture convergence over the Sahel region, shifting the ITCZ southward such that Sahel rainfall decreases[20,96,104] (Fig. 3e). Through this mechanism, the negative AMV during 1960–80 contributed to drying of the Sahel and intensified El Niño-induced droughts. In contrast, the positive AMV since the 1980s promoted convergence of moisture and enhanced rainfall, contributing to Sahel rainfall recovery[96,105], with a large increase in the frequency of extreme rainfall during La Niña[103]. The post-1990 positive AMV phase, conductive to equatorial Pacific easterlies that reinforce the negative IPO[106–108], reinforces the Sahel rainfall recovery and exacerbates the frequency and intensity of extreme rainfall during La Niña.

Modelling ENSO impacts

Although observations allow ENSO impacts on African climate to be examined, model simulations provide greater insight and examination of their changes in the future. Yet modelling such impacts is challenged by the diversity of processes involved. For instance, SST variability across the Pacific, Atlantic and Indian Oceans, and their interactions with each other and the atmosphere, are all integral. The representation of these processes and their bearing on ENSO–Africa climate are now discussed.

Of particular importance is correct simulation of the IOD and its relationship with ENSO. Generally, model representation of ENSO–IOD relationships is poor. Indeed, CMIP6 models[109] show a factor of 5 difference in the amplitude of ENSO and the IOD during SON (Fig. 4a). Models with larger ENSO amplitude systematically produce a stronger IOD amplitude[110,111] (Fig. 4a), with greater ENSO–IOD coupling, in turn, translating into a larger ENSO influence on rainfall average over eastern Africa[5] (Fig. 4b). This influence is highlighted by high spatial coherence in the larger ENSO influence on grid-point rainfall in eastern Africa (Fig. 4c), consistent with the relationship for the east Africa average.

Modelled ENSO relationships with the IOB show similar characteristics. The magnitude of IOB variability during DJF varies by a factor of ~4, and again, those models with a larger ENSO amplitude tend to show a larger IOB amplitude[112,113] (Fig. 4d). In turn, those models with stronger ENSO–IOB coupling systematically generate a greater ENSO-related rainfall response over Africa, notably the dipole pattern between southern and eastern Africa (Fig. 4e,f). The intermodel differences reinforce the importance of the coupling between the Indian and Pacific Ocean SSTs in ENSO-induced rainfall over Africa.

Owing to model inability to reproduce such relationships[7], many models do not accurately simulate ENSO impacts on the African climate. Indeed, model responses are typically weaker and/or less spatially coherent than observed[114] (cf. Fig. 2a–d and Fig. 5a). For example, only ~50% of CMIP6 models simulate a statistically significant correlation between JAS rainfall in the western Sahel and ENSO (Fig. 5a, left). In OND, the impact of ENSO on southern African rainfall is far weaker (cf. Fig. 2b and Fig. 5a, middle left). Furthermore, ENSO's impact on DJF rainfall is concentrated over the western half of southern Africa rather than the eastern half as in observations (cf. Fig. 2c and Fig. 5a, middle right), and its impact on MAM rainfall is weaker than observed.

Simulation of ENSO impacts on African climate is also challenged by underestimation of multidecadal SST variability. Indeed, multiyear rainfall predictability is sourced from the AMV[87,115–117], the IPO[87,115–117], variability in the Indian Ocean and the Mediterranean Sea[20,118], and relative warming of the subtropical North Atlantic with respect to the tropics[119]; for reasons unknown, the majority of models underestimate these sources of multidecadal SST variability[120–123]. This underestimation translates into impact on rainfall, as evidenced by hindcasts of African rainfall variability that correctly simulate the Sahel drought of the 1960s to 1980s and the post-1980s recovery but with a far small amplitude than observed[20,118,124,125]. The underestimated SST variability and the overly weak impact on rainfall mean that their modulation on ENSO–rainfall relationship in Africa is weak, leading to underestimated ENSO-induced droughts and floods.

Projected change in ENSO impact

Knowledge of how ENSO affects the African climate has important implications for understanding and assessing future projections. These projections are invaluable in assessing the potential future impacts of climate change, informing decision-making for adaptation, and increasing resilience to extreme weather events. Although challenged by the difficulty in simulating ENSO–Africa interactions, knowledge of background changes in mean rainfall, and of changes in ENSO and related modes of variability, allows some interpretation of how these relationships could evolve.

Projected mean rainfall changes

Anthropogenically driven changes in climatological rainfall can act to modulate any ENSO-related perturbations: if a changing circulation condition (for example movement of convergence zone and moisture availability) is conducive to a precipitation increase, the same circulation will be conducive to any ENSO-forced increases, exacerbating flooding; if a changing circulation condition is conducive to a precipitation decrease, the same changing circulation will be conducive to any ENSO-forced decreases, exacerbating drought; or ENSO-forced changes could counter any anthropogenic changes. Thus, it is necessary to consider mean rainfall changes.

In the Sahel, mean rainfall is expected to increase under transient greenhouse warming. Indeed, more than 80% of CMIP6 models project an increase in rainfall over central and eastern Sahel (11–15° N, 0–40° E) in all seasons, particularly in JAS (36% increase) and OND (59% increase)[126–130] (Supplementary Fig. 5). These changes arise through various processes, including: an intensified north-minus-south SST gradient[131–133] that favours moisture convergence into the Northern Hemisphere[134]; enhanced land–sea thermal contrasts that intensify the low-level West African Westerly Jet and moisture flux into the Sahel[126,127]; and Mediterranean warming that also promotes

moisture convergence over the Sahel[135]. In the west Sahel, however, rainfall increases are lower, probably owing to a southward shift of the ITCZ[127,129,136,137].

Rainfall is also projected to increase over eastern Africa. In particular, more than 80% of CMIP6 models project an increase in the short rains[138–140], averaging 15% (OND) over all models (Supplementary Fig. 5).

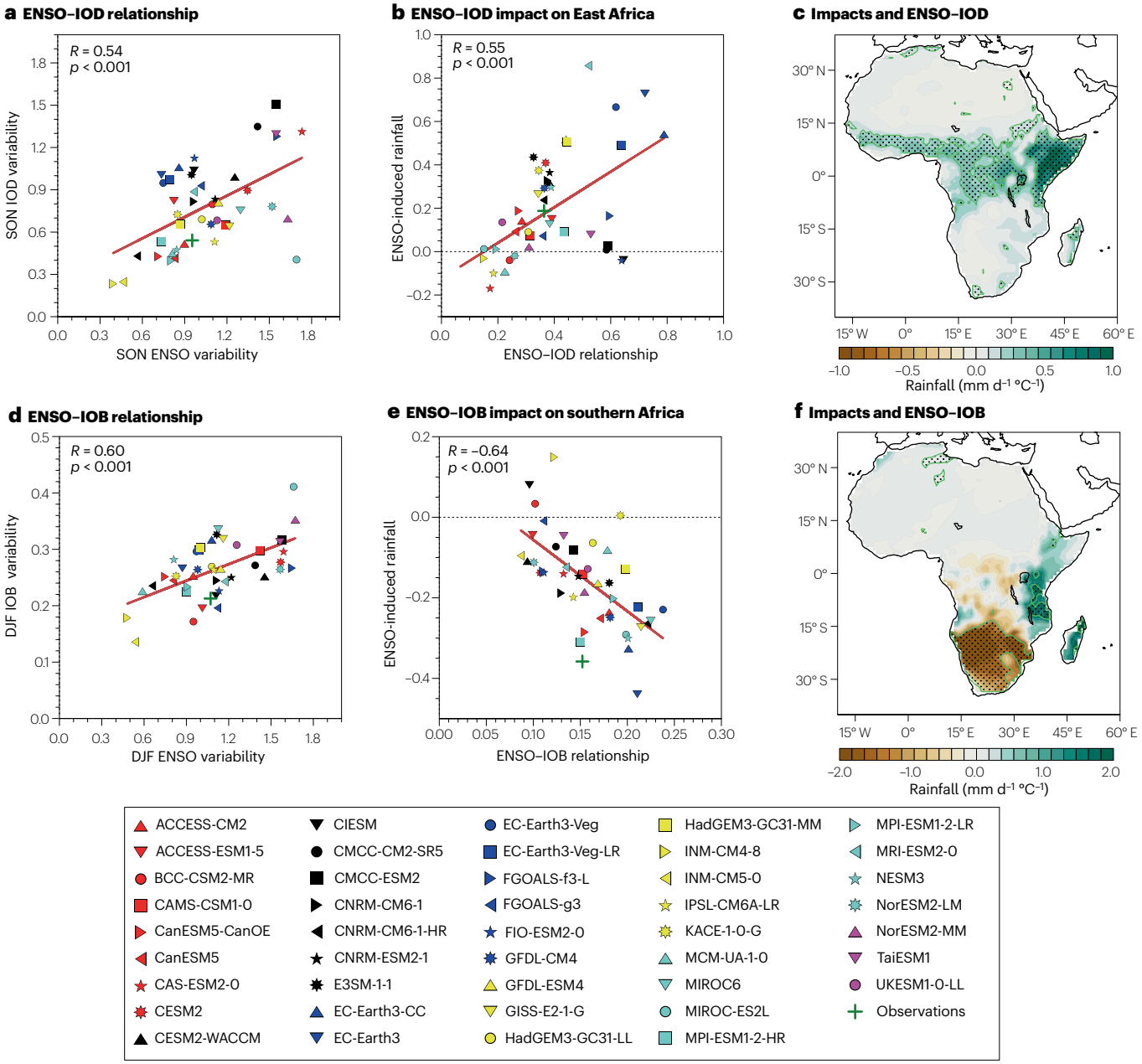

Fig. 4 | IOD and IOB influence on ENSO–African rainfall relationships. **a**, The amplitude of September–October–November (SON) El Niño–Southern Oscillation (ENSO) and Indian Ocean Dipole (IOD; the difference in SST anomalies over the western tropical Indian Ocean (10° S to 10° N, 50–70° E) and the eastern Indian Ocean (10° S to Equator, 90–110° E)) variability in CMIP6 models[109] and their linear fit. Correlation (*R*) and statistical significance (*p*) are displayed at the top left of the plots. **b**, The intermodel relationship between SON ENSO-induced East African (0–10° N, 35–45° E) rainfall and the ENSO–IOD relationship, both defined as the linear regression coefficients between the two variables. **c**, The intermodel relationship between SON ENSO-induced grid-point rainfall anomalies (as the linear regression coefficients of grid-point rainfall anomalies onto the model ENSO index) and the ENSO–IOD relationship (as the linear regression coefficients of the IOD index onto the ENSO index). Stippling represents statistical significance at the 95% confidence level. **d**, As in panel **a**, but the amplitude of December–January–February (DJF) ENSO and Indian Ocean Basin mode (IOB; sea surface temperature anomalies averaged over the tropical Indian Ocean (30° S to 25° N, 40–110° E)) variability. **d**, As in panel **b**, but DJF ENSO-induced rainfall in Southern Africa (15–40° S, 10–40° E) and ENSO–IOB relationship. **f**, As in panel **c**, but for DJF rainfall and DJF IOB. Models in which the IOD and the IOB are more responsive to ENSO produce stronger rainfall anomalies in Africa during ENSO events.

These increases are driven by faster warming in the western equatorial Indian Ocean compared with the eastern Indian Ocean, enhancing convergence over East Africa[110,141,142].

In contrast, rainfall is projected to decrease over southern Africa. For example, robust declines of 25% (JAS), 15% (SON) and 6% (MAM) are projected. These reductions relate to a northward shift of the SICZ[143,144], a northward shift of the Congo Air Boundary[145], an expanding thermal low and a reduced number of tropical lows[145]. In the main rain season of DJF, there is a tendency for a slight rainfall increase but intermodel consensus on the change is low.

Thus, climatological circulation, convergence and moisture availability are changing under greenhouse warming. These changes will affect ENSO impacts. Moreover, changing climatological mean rainfall will offset or exacerbate ENSO impact.

Projected change in modes of SST variability

In addition to changes in mean rainfall, changes in ENSO will greatly influence any resulting impact on Africa. The majority of models project an increase in ENSO SST variability under greenhouse warming. This enhanced SST variability translates into a projected increase in the frequency of strong El Niño and strong La Niña events, swings from a strong El Niño to a strong La Niña event[70,82,146], and disproportionately more frequent multiyear La Niña events than those of strong El Niño events[78]. These changes will translate to more extreme droughts and floods.

As established, other modes of SST variability are also pivotal in ENSO teleconnections to Africa and, hence, will also have a role in determining their future behaviour under warming. Strong pIOD events, for example, are likely to increase in frequency, whereas moderate pIOD events decrease[110,142]. Given that ENSO–IOD relationships are not expected to change[135], these stronger pIOD events could intensify ENSO impact. By contrast, variability of Atlantic Niño/Niña is projected to decrease, and with it the relationship with ENSO[147,148]. This change means that ENSO impact on the Sahel rainfall will be less affected by teleconnection through Atlantic Niño/Niña (which induces a dipole pattern) and more dominated by the tropospheric temperature mechanism (which generates anomalies of the same sign). On interdecadal timescales, the IPO is projected to weaken in amplitude and to shorten in periodicity[149], whereas AMV variance is projected to increase[123]. These changes mean that modulation by the IPO will reduce but that by the AMV will strengthen.

Projected increase in extreme anomalies

Shifts in background rainfall alongside changes in modes of SST variability all translate to an evolution of ENSO–Africa teleconnections in the future. These changes relate to the magnitude and spatial pattern of rainfall impacts, and correspondingly, the frequency of extreme wet and dry events, as now discussed. However, given the tendency for models to underrepresent ENSO–Africa relationships compared with observations[114] (cf. Fig. 3a–d and Fig. 5a), these findings should be interpreted with caution.

Over the Sahel, ENSO–rainfall relationships are projected to strengthen in the future. Recall that in observations, El Niño triggers widespread rainfall reductions across the Sahel during JAS (Fig. 2a) via the troposphere temperature mechanism (Fig. 1a). Although the spatial pattern of rainfall reductions is more constrained in models, it is clear that ENSO's teleconnection here is enhanced in the future (cf. Fig. 5a,b, left). In particular, rainfall sensitivity intensifies and the area of ENSO impacts expands from a small area in the east to also encompass the central and western Sahel (the west boundary from 29° E to 14° E, estimated based on the green contour in Fig. 5a,b, left); these changes are also reproduced when using a subset of models with greater ENSO–IOD coupling or stronger ENSO nonlinearity (Supplementary Figs. 6 and 7). Accordingly, the number of ENSO-related dry seasons increases 63% from 1900–1999 to 2000–2099, and the number of ENSO-related wet seasons increases 135% (Fig. 5c). These changes are consistent with the projected increase in ENSO amplitude and a corresponding increase in the signal-to-noise ratio[68,70], with the larger increase in wet events arising from spatial overlap with the area of increased mean rainfall and a projected increase in La Niña events relative to El Niño (Supplementary Fig. 5a).

ENSO teleconnections also strengthen slightly over East Africa. During OND, historical ENSO-related rainfall anomalies reflect an enhancement (during El Niño) or weakening (during La Niña) of the short rains (Fig. 2b) via interactions with the IOD (Fig. 1b). The magnitude of these anomalies is projected to increase from 0.36 to 0.42 s.d s.d.$^{-1}$ over the East Africa region (5° S to 10° N, 38–50° E) (Fig. 5a,b, middle left). However, the area affected by these ENSO anomalies is little changed. Like for the Sahel, this intensified response is related to the greater signal-to-noise ratio arising from increased ENSO amplitude and the increased mean short rain (Supplementary Fig. 5) that facilitates a stronger response; there is no substantial change in the ENSO–IOD relationship[110]. The smaller amplitude of changes over east Africa during OND relative to the Sahel during JAS translate into smaller changes in wet and dry events. Indeed, the number of short rain seasons with a dry anomaly greater than 1.0 s.d. increases by only 35% (Fig. 5d, left). In comparison, although an increase in wet events is expected with ENSO changes, the total number of seasons with a wet anomaly hardly changes (Fig. 5d, right), owing to an offsetting effect from a decreased frequency of moderate pIOD events coherent with non-extreme El Niño events[142] and the dominant effect of strong El Nino. However, the number of short rain seasons with a wet anomaly greater than a 1.0 s.d. value increases by 37% for strong El Niño events (>1.75 s.d.). The drying signals observed over southern Africa in OND are much weaker in models.

Strengthened ENSO teleconnections are also apparent in DJF under greenhouse warming. In observations, ENSO impacts during this season resemble a dipole between eastern Africa and southern Africa, with the southern lobe dominant (Fig. 2c). Both features are evident in models, albeit with a different spatial configuration. In the future, the wet pole region (eastern Africa during El Niño) is projected to enlarge and be more sensitive (Fig. 5a,b, middle right) due to the projected increase in ENSO amplitude and in mean rainfall (Supplementary Fig. 5). By contrast, the dry pole (southern Africa) shows a small weakening and moderate areal contraction. Accordingly, the number of dry events increases only 10% across southern Africa, amid a 47% increase in wet events (Fig. 5e).

The greater sensitivity of ENSO impacts during DJF also persists into MAM. Historically, El Niño events give rise to drying across southern Africa and minor wetting in east Africa (Fig. 2d). The southern drying remains fairly consistent into the future, but the long rains over east Africa amplify and expand slightly in spatial extent (Fig. 5a,b, right). Given little change in mean rainfall over the region (Supplementary Fig. 5), these shifts are likely to be linked to increased ENSO amplitude that translates to an increased frequency of strong ENSO events. Over eastern Africa, where La Niña or multiyear La Niña induces droughts[16], long rain seasons with a dry and wet anomaly increase by 53% and 20%, respectively (Fig. 5f).

a 1900–1999 Rainfall anomalies associated with ENSO

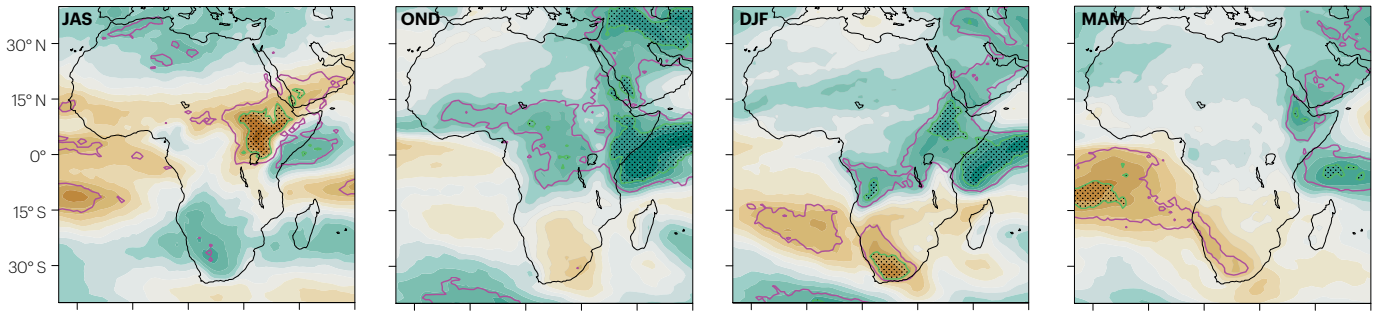

b 2000–2099 Rainfall anomalies associated with ENSO

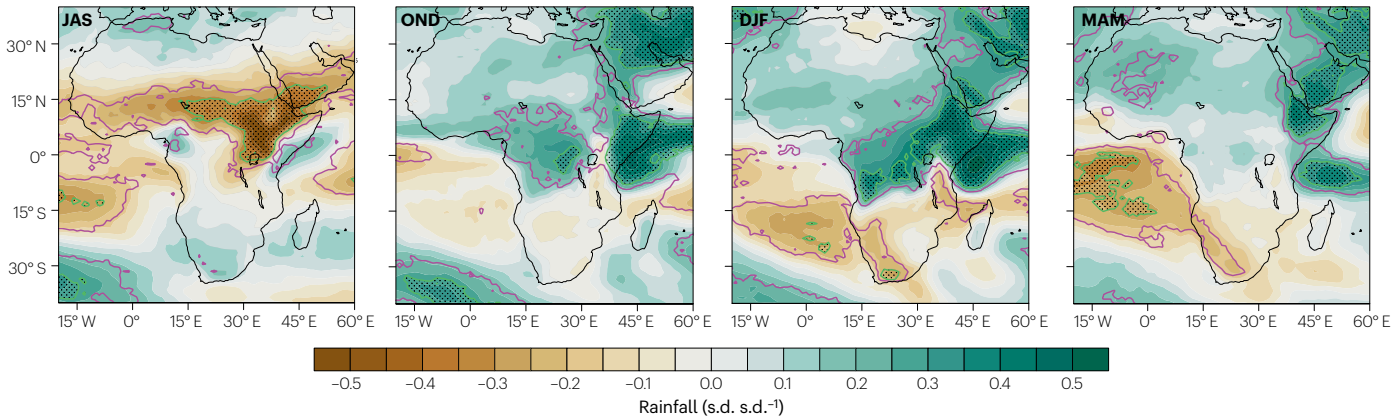

c Evolving ENSO–Sahel JAS rainfall

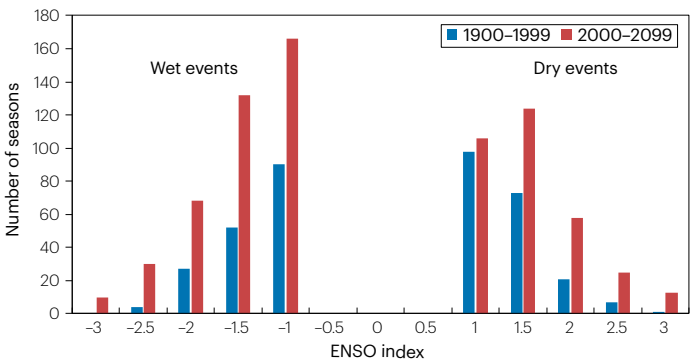

d Evolving ENSO–East Africa OND rainfall

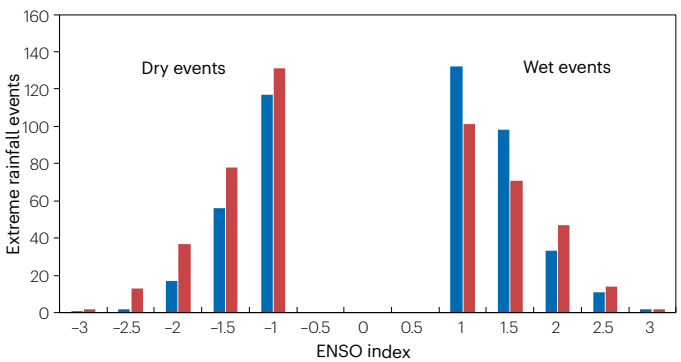

e Evolving ENSO–southern Africa DJF rainfall

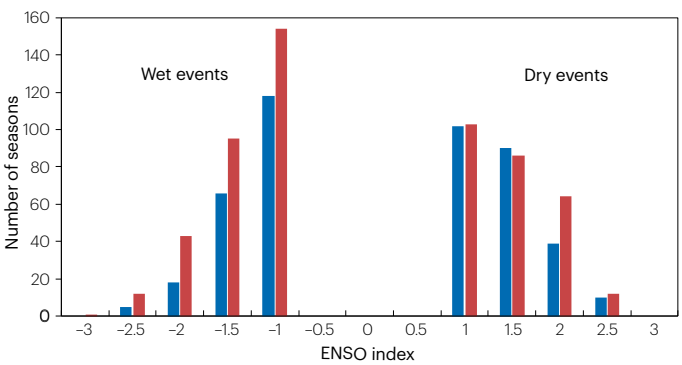

f Evolving ENSO–East Africa MAM rainfall

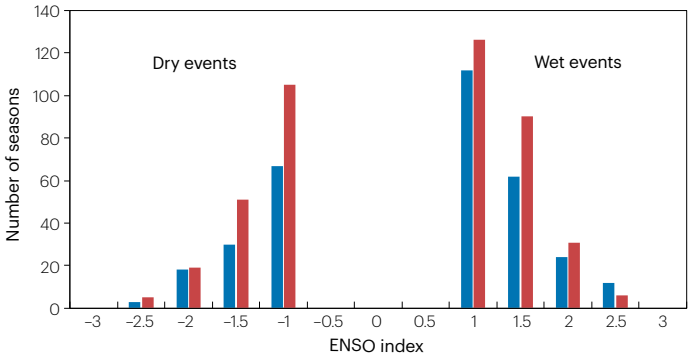

Fig. 5 | Future change of African rainfall associated with ENSO. a, Multimodel ensemble mean regression of normalized rainfall anomalies onto the normalized Niño3.4 index from CMIP6 models over 1900–1999 for July–August–September (JAS), October–November–December (OND), December–January–February (DJF) and March–April–May (MAM); purple and green contours indicate where more than 50% and 70% of models agree on a rainfall decrease during El Niño, respectively, and stippling where correlations are significant above the 95% confidence level. **b**, As in panel **a**, but for 2000–2099. In panels **a** and **b**, seasonal rainfall anomalies and Niño3.4 are quadratically detrended and normalized over the 1900–2099 period for each model and then separated into the two 100-year periods. **c**, The number of wet (rainfall anomalies >1.0 s.d.) and dry (rainfall anomalies <−1.0 s.d.) seasons in the Sahel (17° W to 40° E, 11–15° N) during JAS by El Niño–Southern Oscillation (ENSO) amplitude in 1900–1999 (blue) and 2000–2099 (red). **d**, As in panel **c**, but for OND rainfall in East Africa (35–55° E, 12° S to 25° N). **e**, As in panel **c**, but for DJF rainfall in southern Africa (15–40° S, 10–40° E). **f**, As in panel **c**, but MAM rainfall in East Africa. In general, increased ENSO variability leads to a higher frequency of dry and wet extreme anomalies in the future.

Summary and future perspectives

ENSO exerts a substantial impact on the African climate. It does so by forcing anomalies in the tropical troposphere, driving tropical SST variability that interacts with ENSO, inducing extratropical oceanic and atmospheric anomalies, and changing regional circulations. These contrasting drivers translate into marked variability in resulting precipitation impacts that historically include: anomalies over the Sahel during JAS; a dipole in anomalies between eastern and southern Arica during OND and DJF; and a weak dipole between southern Africa and eastern Africa during MAM. However, ENSO-related climate impacts are challenging to generalize, owing to event asymmetry, differences between El Niño and La Niña, as well as modulation by multidecadal variability. Complex atmosphere–ocean interactions across multiple basins complicate simulation of these teleconnections. Nevertheless, under transient greenhouse warming, ENSO-induced dry and wet anomalies are expected to increase over much of Africa, manifesting as an increased frequency of both dry and wet extremes.

Simulation of ENSO–Africa teleconnections is challenging and uncertain, highlighting a research focus. There are many longstanding model systematic errors and biases that probably have a substantial impact on historical and future simulation of ENSO–Africa relationships: those pertaining to simulation of ENSO (cold bias in the equatorial central Pacific[150], overly strong easterly winds and overly cool SST and overly shallow thermocline in the equatorial eastern Indian Ocean[110,151], and a warm bias in the eastern boundary current system regions of the tropical Pacific and Atlantic[107]); those pertaining to simulation of rains in Africa (overly strong short rains[100,139] and overly strong summer rainfall over southern Africa[114]); and those pertaining to ENSO interbasin interactions (weak ENSO–IOD coupling[110,114] and ENSO–Atlantic Niño/Niña interactions[148,152]). Impacts from some of the biases remain unknown, particularly their relevance to African teleconnections.

High-resolution models are urgently required to address many of the biases. Vertical heat transport by submesoscale oceanic eddies (<10 km in the tropics), simulated only in high-resolution models, leads to marked alleviation of the cold bias in the equatorial central Pacific and improved ENSO properties[153]. It is likely that submesoscale eddy could also alleviate biases of the overly cool SST and shallow thermocline in the equatorial eastern Indian Ocean, reducing the IOD amplitude that is responsible for the IOD being too independent of ENSO, and improving ENSO–IOD interactions and ENSO impacts on Africa. High resolution is also urgently required to simulate regional circulation and regional rainfall[154], including the Angola Low, Tropical Temperate Trough events and the SICZ. Initiatives such as coordinated regional climate downscaling experiments (CORDEX)[154] can be effective as they allow regional processes crucial for the simulation of extreme events[155–157]. However, these simulations, when using outputs of low-resolution global models as boundary conditions, inherit biases from the global models[158] (including the bias in east Africa rainfall seasonality[155]), further highlighting the need to rectify global model errors by using high-resolution models.

In addition to model development and increased access to high-resolution models, there are also several knowledge gaps that require investigation. Most projections compare differences between the twenty-first and the twentieth centuries, assuming a unidirectional or linear change as greenhouse warming proceeds. However, even under a persistent increase in CO_2 beyond 2100 as in the SSP5-8.5 emission scenario[109], the response of ENSO might not be unidirectional or linear. For example, in a limited number of models that are integrated beyond 2100, ENSO undergoes an initial increase and a subsequent reduction[159,160]. Whether ENSO impact on Africa also evolves nonlinearly depends on competing factors, for example a decreased ENSO amplitude versus an increased sensitivity arising from mean rainfall changes and rising temperatures. An increased number of models that integrate beyond 2100 is needed to aid a comprehensive assessment of the likely nonlinear behaviour of ENSO and its impacts on Africa.

Another knowledge gap is interactions on synoptic timescales between mean climate change, such as high temperature and atmospheric moisture, and ENSO anomalies. At present, analysis is mostly conducted on seasonal or monthly averages. How mean climate change manifests on weather timescales, or how it interacts with ENSO-induced extreme weather, is unclear. There is evidence suggesting that climate change amplifies ENSO-related extreme events, for example the severity of drought during the 2015/16 El Niño[161]. Continuous daily outputs of climate simulations, preferably from high-resolution climate models, are needed to address the issue.

Given the important influence of ENSO on the African climate, and the resulting socioeconomic impacts of ENSO-related climate variability, these limitations must be addressed. Doing so will improve assessment of the maximum range of potential risks, essential for forecasting and early warming, improved adaptation, and assessment of mitigation strategies. Such actions are vital to limit the extreme socioeconomic consequences of ENSO across the African continent, helping to reduce food shortages, prevent famine and eliminate premature deaths.

Published online: 5 August 2025

References

1. Saji, N. H., Goswami, B. N., Vinayachandran, P. N. & Yamagata, T. A dipole mode in the tropical Indian Ocean. *Nature* **401**, 360–363 (1999).
2. Palmer, P. I. et al. Drivers and impacts of eastern African rainfall variability. *Nat. Rev. Earth Environ.* **4**, 254–270 (2023).
3. Klein, S. A., Soden, B. J. & Lau, N. C. Remote sea surface temperature variations during ENSO: evidence for a tropical atmospheric bridge. *J. Clim.* **12**, 917–932 (1999).
4. Latif, M. & Grötzner, A. The equatorial Atlantic oscillation and its response to ENSO. *Clim. Dyn.* **16**, 213–218 (2000).
5. Goddard, L. & Graham, N. E. Importance of the Indian Ocean for simulating rainfall anomalies over eastern and southern Africa. *J. Geophys. Res.* **104**, 19099–19116 (1999).
6. Rodríguez-Fonseca, B. et al. Interannual and decadal SST-forced responses of the West African monsoon. *Atmos. Sci. Lett.* **12**, 67–74 (2011).

7. Cai, W. et al. Pantropical climate interactions. *Science* **363**, eaav4236 (2019).
8. Halpern, D. & Woiceshyn, P. M. Somali Jet in the Arabian Sea, El Niño, and India rainfall. *J. Clim.* **14**, 434–441 (2001).
9. Howard, E. & Washington, R. Characterizing the synoptic expression of the Angola Low. *J. Clim.* **31**, 7147–7165 (2018).
10. Cook, K. H. The south Indian convergence zone and interannual rainfall variability over southern Africa. *J. Clim.* **13**, 3789–3804 (2000).
11. Howard, E. & Washington, R. Drylines in southern Africa: rediscovering the Congo air boundary. *J. Clim.* **32**, 8223–8242 (2019).
12. Hart, N. C. G., Reason, C. J. C. & Fauchereau, N. Cloud bands over southern Africa: seasonality, contribution to rainfall variability and modulation by the MJO. *Clim. Dyn.* **41**, 1199–1212 (2013).
13. Macron, C., Pohl, B., Richard, Y. & Bessafi, M. How do tropical temperate troughs form and develop over southern Africa? *J. Clim.* **27**, 1633–1647 (2014).
14. Webster, P. J., Moore, A. M., Loschnigg, J. P. & Leben, R. R. Coupled ocean–atmosphere dynamics in the Indian Ocean during 1997–98. *Nature* **401**, 356–360 (1999).
15. Hashizume, M., Chaves, L. F. & Minakawa, N. Indian Ocean Dipole drives malaria resurgence in East African highlands. *Sci. Rep.* **2**, 269 (2012).
16. Funk, C. et al. Examining the role of unusually warm Indo-Pacific sea-surface temperatures in recent African droughts. *Q. J. R. Meteorol. Soc.* **144**, 360–383 (2018).
17. Kimutai, J. B. et al. *Human-Induced Climate Change Increased Drought Severity in Horn of Africa*. UNU-EHS Working Paper https://doi.org/10.25561/103482 (Imperial College London, 2023).
18. Nicholson, S. E. The West African Sahel: a review of recent studies on the rainfall regime and its interannual variability. *ISRN Meteorol.* **2013**, 1–32 (2013).
19. Lintner, B. R. & Chiang, J. C. H. Reorganization of tropical climate during El Nino: a weak temperature gradient approach. *J. Clim.* **18**, 5312–5329 (2005).
20. Sheen, K. L. et al. Skilful prediction of Sahel summer rainfall on inter-annual and multi-year timescales. *Nat. Commun.* **8**, 14966 (2017).
21. Rowell, D. P. Teleconnections between the tropical Pacific and the Sahel. *Q. J. R. Meteorol. Soc.* **127**, 1683–1706 (2001).
22. Gleixner, S., Keenlyside, N., Viste, E. & Korecha, D. The El Niño effect on Ethiopian summer rainfall. *Clim. Dyn.* **49**, 1865–1883 (2017).
23. Diro, G. T., Grimes, D. I. F. & Black, E. Teleconnections between Ethiopian summer rainfall and sea surface temperature: part I — observation and modelling. *Clim. Dyn.* **37**, 103–119 (2011).
24. Janicot, S., Trzaska, S. & Poccard, I. Summer Sahel–ENSO teleconnection and decadal time scale SST variations. *Clim. Dyn.* **18**, 303–320 (2001).
25. Joly, M. & Voldoire, A. Influence of ENSO on the West African monsoon: temporal aspects and atmospheric processes. *J. Clim.* **22**, 3193–3210 (2009).
26. Weller, E. et al. More-frequent extreme northward shifts of eastern Indian Ocean tropical convergence under greenhouse warming. *Sci. Rep.* **4**, 6087 (2014).
27. Black, E., Slingo, J. & Sperber, K. R. An observational study of the relationship between excessively strong short rains in coastal East Africa and Indian Ocean SST. *Mon. Wea. Rev.* **131**, 74–94 (2003).
28. Moihamette, F., Pokam, W. M., Diallo, I. & Washington, R. Extreme Indian Ocean Dipole and rainfall variability over central Africa. *Int. J. Climatol.* **42**, 5255–5272 (2022).
29. Lindesay, J. A., Harrison, M. S. J. & Haffner, M. P. The Southern Oscillation and South African rainfall. *S. Afr. J. Sci.* **82**, 196–198 (1986).
30. Blamey, R. C., Kolusu, S. R., Mahlalela, P., Todd, M. C. & Reason, C. J. C. The role of regional circulation features in regulating El Nino climate impacts over southern Africa: a comparison of the 2015/2016 drought with previous events. *Int. J. Climatol.* **38**, 4276–4295 (2018).
31. Rodríguez-Fonseca, B. et al. Variability and predictability of West African droughts: a review on the role of sea surface temperature anomalies. *J. Clim.* **28**, 4034–4060 (2015).
32. Reason, C. J. C. The Bolivian, Botswana, and Bilybara highs and Southern Hemisphere drought/floods. *Geophys. Res. Lett.* **43**, 1280–1286 (2016).
33. Hart, N. C. G., Washington, R. & Reason, C. J. C. On the likelihood of tropical–extratropical cloud bands in the South Indian convergence zone during ENSO events. *J. Clim.* **31**, 2797–2817 (2018).
34. Barimalala, R., Blamey, R. C., Desbiolles, F. & Reason, C. J. C. Variability in the Mozambique Channel Trough and impacts on southeast African rainfall. *J. Clim.* **33**, 749–765 (2020).
35. Reason, C. J. C. Subtropical Indian Ocean SST dipole events and southern African rainfall. *Geophys. Res. Lett.* **28**, 2225–2227 (2001).
36. Behera, S. K. & Yamagata, T. Subtropical SST dipole events in the southern Indian Ocean. *Geophys. Res. Lett.* **28**, 327–330 (2001).
37. Fauchereau, N., Trzaska, S., Richard, Y., Roucou, P. & Camberlin, P. Sea-surface temperature co-variability in the southern Atlantic and Indian Oceans and its connections with the atmospheric circulation in the Southern Hemisphere. *Int. J. Climatol.* **23**, 663–677 (2003).
38. Chang, P., Fang, Y., Saravanan, R., Ji, L. & Seidel, H. The cause of the fragile relationship between the Pacific El Nino and the Atlantic Nino. *Nature* **443**, 324–328 (2006).
39. Giannini, A., Saravanan, R. & Chang, P. Oceanic forcing of Sahel rainfall on interannual to interdecadal time scales. *Science* **302**, 1027–1030 (2003).
40. de, Oliveira, C. P., Aímola, L., Ambrizzi, T. & Freitas, A. C. V. The influence of the regional Hadley and Walker circulations on precipitation patterns over Africa in El Niño, La Niña, and neutral years. *Pure Appl. Geophys.* **175**, 2293–2306 (2018).
41. Xie, S. P. & Carton, J. A. Tropical atlantic variability: patterns, mechanisms, and impacts. *Am. Geophys. Union.* **147**, 121–142 (2004).
42. Pomposi, C., Giannini, A., Kushnir, Y. & Lee, D. E. Understanding Pacific Ocean influence on interannual precipitation variability in the Sahel. *Geophys. Res. Lett.* **43**, 9234–9242 (2016).
43. Rowell, D. P. The impact of Mediterranean SSTs on the Sahelian rainfall season. *J. Clim.* **16**, 849–862 (2003).
44. Fontaine, B. et al. Impacts of warm and cold situations in the Mediterranean basins on the West African monsoon: observed connection patterns (1979–2006) and climate simulations. *Clim. Dyn.* **35**, 95–114 (2010).
45. Thompson, D. W. J. & Wallace, J. M. Annular modes in the extratropical circulation. Part I: Month-to-month variability. *J. Clim.* **13**, 1000–1016 (2000).
46. Reason, C. J. C. & Rouault, M. Links between the Antarctic oscillation and winter rainfall over western South Africa. *Geophys. Res. Lett.* **32**, L07705 (2005).
47. Mahlalela, P. T., Blamey, R. C., Hart, N. C. G. & Reason, C. J. C. Drought in the Eastern Cape region of South Africa and trends in rainfall characteristics. *Clim. Dyn.* **55**, 2743–2759 (2020).
48. Lavaysse, C., Flamant, C. & Janicot, S. Regional-scale convection patterns during strong and weak phases of the Saharan heat low. *Atmos. Sci. Lett.* **11**, 255–264 (2010).
49. Lavaysse, C., Flamant, C., Evan, A., Janicot, S. & Gaetani, M. Recent climatological trend of the Saharan heat low and its impact on the West African climate. *Clim. Dyn.* **47**, 3479–3498 (2016).
50. Thorncroft, C. D. & Blackburn, M. Maintenance of the African easterly jet. *Q. J. R. Meteorol. Soc.* **125**, 763–786 (1999).
51. Riddle, E. E. & Cook, K. H. Abrupt rainfall transitions over the Greater Horn of Africa: observations and regional model simulations. *J. Geophys. Res.* **113**, D15109 (2008).
52. Iqbal, W. et al. Mean climate and representation of jet streams in the CORDEX South Asia simulations by the regional climate model RCA4. *Theor. Appl. Climatol.* **129**, 1–19 (2017).
53. Vizy, E. K. & Cook, K. H. Connections between the summer East African and Indian rainfall regimes. *J. Geophys. Res.* **108**, 4510 (2003).
54. Jain, S., Mishra, S. K., Anand, A., Salunke, P. & Fasullo, J. T. Historical and projected low-frequency variability in the Somali Jet and Indian summer monsoon. *Clim. Dyn.* **56**, 749–765 (2021).
55. Crétat, J., Pohl, B., Dieppois, B., Berthou, S. & Pergaud, J. The Angola Low: relationship with southern African rainfall and ENSO. *Clim. Dyn.* **52**, 1783–1803 (2019).
56. Reason, C. J. C. et al. A review of South African research in atmospheric science and physical oceanography during 2000–2005: review article. *S. Afr. J. Sci.* **102**, 35–45 (2006).
57. Driver, P. & Reason, C. J. C. Variability in the Botswana High and its relationships with rainfall and temperature characteristics over southern Africa. *Int. J. Climatol.* **37**, 570–581 (2017).
58. Maoyi, M. L. & Abiodun, B. J. How well does MPAS-atmosphere simulate the characteristics of the Botswana High? *Clim. Dyn.* **57**, 2109–2128 (2021).
59. Todd, M. & Washington, R. Circulation anomalies associated with tropical-temperate troughs in southern Africa and the south west Indian Ocean. *Clim. Dyn.* **15**, 937–951 (1999).
60. Pohl, B., Fauchereau, N., Richard, Y., Rouault, M. & Reason, C. J. C. Interactions between synoptic, intraseasonal and interannual convective variability over southern Africa. *Clim. Dyn.* **33**, 1033–1050 (2009).
61. Manhique, A. J., Reason, C. J. C., Rydberg, L. & Fauchereau, N. ENSO and Indian Ocean sea surface temperatures and their relationships with tropical temperate troughs over Mozambique and the southwest Indian Ocean. *Int. J. Climatol.* **31**, 1–13 (2011).
62. Hart, N. C. G., Reason, C. J. C. & Fauchereau, N. Tropical–extratropical interactions over southern Africa: three cases of heavy summer season rainfall. *Mon. Wea. Rev.* **138**, 2608–2623 (2010).
63. Lazenby, M. J., Todd, M. C. & Wang, Y. Climate model simulation of the South Indian Ocean convergence zone: mean state and variability. *Clim. Res.* **68**, 59–71 (2016).
64. Barimalala, R., Desbiolles, F., Blamey, R. C. & Reason, C. Madagascar influence on the South Indian Ocean convergence zone, the Mozambique Channel Trough and southern African rainfall. *Geophys. Res. Lett.* **45**, 11,380–311,389 (2018).
65. Kug, J. S., Jin, F. F. & An, S.-I. Two types of El Niño Events: cold tongue El Niño and warm pool El Niño. *J. Clim.* **22**, 1499–1515 (2009).
66. Takahashi, K., Montecinos, A., Goubanova, K. & Dewitte, B. ENSO regimes: reinterpreting the canonical and Modoki El Niño. *Geophys. Res. Lett.* **38**, L10704 (2011).
67. Capotondi, A. et al. Understanding ENSO diversity. *Bull. Am. Meteorol. Soc.* **96**, 921–938 (2015).
68. Cai, W. et al. ENSO and greenhouse warming. *Nat. Clim. Change* **5**, 849–859 (2015).
69. Cai, W. et al. Increased variability of eastern Pacific El Niño under greenhouse warming. *Nature* **564**, 201–206 (2018).
70. Cai, W. et al. Changing El Nino–Southern Oscillation in a warming climate. *Nat. Rev. Earth Environ.* **2**, 628–644 (2021).
71. Frauen, C., Dommenget, D., Tyrrell, N., Rezny, M. & Wales, S. Analysis of the nonlinearity of El Niño–Southern Oscillation teleconnections. *J. Clim.* **27**, 6225–6244 (2014).
72. Cai, W. et al. Increased frequency of extreme La Niña events under greenhouse warming. *Nat. Clim. Change* **5**, 132–137 (2015).
73. Takahashi, K. & Dewitte, B. Strong and moderate nonlinear El Niño regimes. *Clim. Dyn.* **46**, 1627–1645 (2016).
74. Bader, J. & Latif, M. The 1983 drought in the West Sahel: a case study. *Clim. Dyn.* **36**, 463–472 (2011).
75. Jia, F., Cai, W., Gan, B., Wu, L. & Di Lorenzo, E. Enhanced North Pacific impact on El Niño/Southern Oscillation under greenhouse warming. *Nat. Clim. Change* **11**, 840–847 (2021).

76. Ratnam, J. V., Behera, S. K., Masumoto, Y. & Yamagata, T. Remote effects of El Niño and Modoki events on the Austral summer precipitation of southern Africa. *J. Clim.* **27**, 3802–3815 (2014).
77. *Southern Africa Drought* (WFP, 2025); https://www.wfp.org/emergencies/southern-africa-drought.
78. Geng, T. et al. Increased occurrences of consecutive La Nina events under global warming. *Nature* **619**, 774–781 (2023).
79. Richard, Y., Trzaska, S., Roucou, P. & Rouault, M. Modification of the Southern African rainfall variability/ENSO relationship since the late 1960s. *Clim. Dyn.* **16**, 883–895 (2000).
80. Clark, C. O., Webster, P. J. & Cole, J. E. Interdecadal variability of the relationship between the Indian Ocean zonal mode and East African coastal rainfall anomalies. *J. Clim.* **16**, 548–554 (2003).
81. Kim, S. T. et al. Response of El Niño sea surface temperature variability to greenhouse warming. *Nat. Clim. Change* **4**, 786–790 (2014).
82. Cai, W. et al. Anthropogenic impacts on twentieth-century ENSO variability changes. *Nat. Rev. Earth Environ.* **4**, 407–418 (2023).
83. Pomposi, C., Kushnir, Y., Giannini, A. & Biasutti, M. Toward understanding the occurrence of both wet and dry Sahel seasons during El Nino: the modulating role of the global ocean. *J. Clim.* **33**, 1193–1207 (2020).
84. Suárez-Moreno, R., Rodríguez-Fonseca, B., Barroso, J. A. & Fink, A. H. Interdecadal changes in the leading ocean forcing of Sahelian rainfall interannual variability: atmospheric dynamics and role of multidecadal SST background. *J. Clim.* **31**, 6687–6710 (2018).
85. Ham, Y. G., Kug, J. S. & Park, J. Y. Two distinct roles of Atlantic SSTs in ENSO variability: North Tropical Atlantic SST and Atlantic Nino. *Geophys. Res. Lett.* **40**, 4012–4017 (2013).
86. Nnamchi, H. C., Dike, V. N., Akinsanola, A. A. & Okoro, U. K. Leading patterns of the satellite-era summer precipitation over West Africa and associated global teleconnections. *Atmos. Res.* **259**, 105677 (2021).
87. Mohino, E., Keenlyside, N. & Pohlmann, H. Decadal prediction of Sahel rainfall: where does the skill (or lack thereof) come from? *Clim. Dyn.* **47**, 3593–3612 (2016).
88. Losada, T. et al. Tropical SST and Sahel rainfall: a non-stationary relationship. *Geophys. Res. Lett.* **39**, L12705 (2012).
89. Ashok, K., Guan, Z. Y. & Yamagata, T. A look at the relationship between the ENSO and the Indian Ocean Dipole. *J. Meteor. Soc. Jpn.* **81**, 41–56 (2003).
90. Kebacho, L. L. Large-scale circulations associated with recent interannual variability of the short rains over East Africa. *Meteorol. Atmos. Phys.* **134**, 10 (2022).
91. Ham, Y. G., Choi, J. Y. & Kug, J. S. The weakening of the ENSO–Indian Ocean Dipole (IOD) coupling strength in recent decades. *Clim. Dyn.* **49**, 249–261 (2017).
92. Manatsa, D., Mukwada, G. & Makaba, L. ENSO shifts and their link to southern Africa surface air temperature in summer. *Theor. Appl. Climatol.* **132**, 727–738 (2018).
93. Hoell, A., Funk, C., Zinke, J. & Harrison, L. Modulation of the Southern Africa precipitation response to the El Niño Southern Oscillation by the subtropical Indian Ocean Dipole. *Clim. Dyn.* **48**, 2529–2540 (2017).
94. Wang, S. S., Huang, J. P., He, Y. L. & Guan, Y. P. Combined effects of the Pacific Decadal Oscillation and El Nino–Southern Oscillation on global land dry-wet changes. *Sci. Rep.* **4**, 6651 (2014).
95. Villamayor, J. & Mohino, E. Robust Sahel drought due to the Interdecadal Pacific Oscillation in CMIP5 simulations. *Geophys. Res. Lett.* **42**, 1214–1222 (2015).
96. Mohino, E., Janicot, S. & Bader, J. Sahel rainfall and decadal to multi-decadal sea surface temperature variability. *Clim. Dyn.* **37**, 419–440 (2011).
97. Mason, S. J. El Nino, climate change, and southern African climate. *Environ* **12**, 327–345 (2001).
98. Malherbe, J., Dieppois, B., Maluleke, P., Van Staden, M. & Pillay, D. L. South African droughts and decadal variability. *Nat. Hazards* **80**, 657–681 (2016).
99. Liebmann, B. et al. Climatology and interannual variability of boreal spring wet season precipitation in the eastern Horn of Africa and implications for its recent decline. *J. Clim.* **30**, 3867–3886 (2017).
100. Funk, C. et al. Warming of the Indian Ocean threatens eastern and southern African food security but could be mitigated by agricultural development. *P. Natl. Acad. Sci. USA* **105**, 11081–11086 (2008).
101. Yang, W. C., Seager, R., Cane, M. A. & Lyon, B. The East African long rains in observations and models. *J. Clim.* **27**, 7185–7202 (2014).
102. Lyon, B. Seasonal drought in the Greater Horn of Africa and its recent increase during the March–May long rains. *J. Clim.* **27**, 7953–7975 (2014).
103. Badji, A., Mohino, E., Diakhate, M., Mignot, J. & Gaye, A. T. Decadal variability of rainfall in Senegal: beyond the total seasonal amount. *J. Clim.* **35**, 5339–5358 (2022).
104. Hoerling, M., Hurrell, J., Eischeid, J. & Phillips, A. Detection and attribution of twentieth-century northern and southern African rainfall change. *J. Clim.* **19**, 3989–4008 (2006).
105. Zhang, R. & Delworth, T. L. Impact of Atlantic multidecadal oscillations on India/Sahel rainfall and Atlantic hurricanes. *Geophys. Res. Lett.* **33**, L17712 (2006).
106. Ruprich-Robert, Y. et al. Assessing the climate impacts of the observed Atlantic multidecadal variability using the GFDL CM2.1 and NCAR CESM1 global coupled models. *J. Clim.* **30**, 2785–2810 (2017).
107. McGregor, S. et al. Recent Walker circulation strengthening and Pacific cooling amplified by Atlantic warming. *Nat. Clim. Change* **4**, 888–892 (2014).
108. Li, X. C., Xie, S. P., Gille, S. T. & Yoo, C. Atlantic-induced pan-tropical climate change over the past three decades. *Nat. Clim. Change* **6**, 275–279 (2016).
109. Eyring, V. et al. Overview of the Coupled Model Intercomparison Project phase 6 (CMIP6) experimental design and organization. *Geosci. Model. Dev.* **9**, 1937–1958 (2016).
110. Wang, G. et al. The Indian Ocean Dipole in a warming world. *Nat. Rev. Earth Environ.* **5**, 588–604 (2024).
111. Cai, W., Sullivan, A. & Cowan, T. Interactions of ENSO, the IOD, and the SAM in CMIP3 models. *J. Clim.* **24**, 1688–1704 (2011).
112. Tao, W. et al. Interdecadal modulation of ENSO teleconnections to the Indian Ocean Basin Mode and their relationship under global warming in CMIP5 models. *Int. J. Climatol.* **35**, 391–407 (2015).
113. Zheng, X.-T., Xie, S.-P. & Liu, Q. Response of the Indian Ocean Basin Mode and its capacitor effect to global warming. *J. Clim.* **24**, 6146–6164 (2011).
114. Dieppois, B., Rouault, M. & New, M. The impact of ENSO on southern African rainfall in CMIP5 ocean atmosphere coupled climate models. *Clim. Dyn.* **45**, 2425–2442 (2015).
115. Gaetani, M. & Mohino, E. Decadal prediction of the Sahelian precipitation in CMIP5 simulations. *J. Clim.* **26**, 7708–7719 (2013).
116. García-Serrano, J., Guemas, V. & Doblas-Reyes, F. J. Added-value from initialization in predictions of Atlantic multi-decadal variability. *Clim. Dyn.* **44**, 2539–2555 (2015).
117. Bellucci, A. et al. An assessment of a multi-model ensemble of decadal climate predictions. *Clim. Dyn.* **44**, 2787–2806 (2015).
118. He, Y. J. et al. Role of ocean initialization in skillful prediction of Sahel rainfall on the decadal time scale. *J. Clim.* **36**, 2109–2129 (2023).
119. Martin, E. R. & Thorncroft, C. Sahel rainfall in multimodel CMIP5 decadal hindcasts. *Geophys. Res. Lett.* **41**, 2169–2175 (2014).
120. Du, Y. & Chen, H. Evaluation of CMIP6 model performance in simulating the PDO and its future change. *Atmos. Ocean. Sci. Lett.* **17**, 100449 (2024).
121. Xu, M., Xu, Y., Li, T., Shen, S. & Hu, Z. Evaluation of the Pacific decadal oscillation from 1901 to 2014 in CMIP6 models. *Clim. Res.* **90**, 1–15 (2023).
122. Ma, Y., Yuan, N., Dong, T. & Dong, W. On the Pacific decadal oscillation simulations in CMIP6 models: a new test-bed from climate network analysis. *Asia-Pac. J. Atmos. Sci.* **59**, 17–28 (2023).
123. Li, S. et al. Intensified Atlantic multidecadal variability in a warming climate. *Nat. Clim. Change* **15**, 293–300 (2025).
124. Zanna, L. Forecast skill and predictability of observed Atlantic sea surface temperatures. *J. Clim.* **25**, 5047–5056 (2012).
125. Yeager, S. G. et al. Predicting near-term changes in the Earth system: a large ensemble of initialized decadal prediction simulations using the Community Earth System Model. *Bull. Am. Meteorol. Soc.* **99**, 1867–1886 (2018).
126. Haarsma, R. J., Selten, F. M., Weber, S. L. & Kliphuis, M. Sahel rainfall variability and response to greenhouse warming. *Geophys. Res. Lett.* **32**, L17702 (2005).
127. Vizy, E. K., Cook, K. H., Crétat, J. & Neupane, N. Projections of a wetter Sahel in the twenty-first century from global and regional models. *J. Clim.* **26**, 4664–4687 (2013).
128. Almazroui, M. et al. Projected change in temperature and precipitation over Africa from CMIP6. *Earth Syst. Environ.* **4**, 455–475 (2020).
129. Monerie, P.-A., Sanchez-Gomez, E., Gaetani, M., Mohino, E. & Dong, B. Future evolution of the Sahel precipitation zonal contrast in CESM1. *Clim. Dyn.* **55**, 2801–2821 (2020).
130. Zhang, Z. & Li, G. Uncertainty in the projected changes of Sahel summer rainfall under global warming in CMIP5 and CMIP6 multi-model ensembles. *Clim. Dyn.* **59**, 3579–3597 (2022).
131. Monerie, P.-A., Pohl, B. & Gaetani, M. The fast response of Sahel precipitation to climate change allows effective mitigation action. *npj Clim. Atmos. Sci.* **4**, 24 (2021).
132. Cai, W. et al. Southern Ocean warming and its climatic impacts. *Sci. Bull.* **68**, 946–960 (2023).
133. IPCC: Summary for Policymakers. In *Climate Change 2021: The Physical Science Basis* (eds Masson-Delmotte, V. et al.) 3–32 (Cambridge Univ. Press, 2021).
134. Guilbert, M., Terray, P., Mignot, J., Ollier, L. & Gastineau, G. Interhemispheric temperature gradient and equatorial Pacific SSTs drive Sahel monsoon uncertainties under global warming. *J. Clim.* **37**, 1033–1052 (2024).
135. Park, J.-y, Bader, J. & Matei, D. Anthropogenic Mediterranean warming essential driver for present and future Sahel rainfall. *Nat. Clim. Change* **6**, 941–945 (2016).
136. Gaetani, M. et al. West African monsoon dynamics and precipitation: the competition between global SST warming and CO_2 increase in CMIP5 idealized simulations. *Clim. Dyn.* **48**, 1353–1373 (2017).
137. Paeth, H. & Hense, A. SST versus climate change signals in West African rainfall: 20th-century variations and future projections. *Clim. Change* **65**, 179–208 (2004).
138. Shongwe, M. E., van Oldenborgh, G. J., van den Hurk, B. & van Aalst, M. Projected changes in mean and extreme precipitation in Africa under global warming. Part II: East Africa. *J. Clim.* **24**, 3718–3733 (2011).
139. Tierney, J. E., Ummenhofer, C. C. & deMenocal, P. B. Past and future rainfall in the Horn of Africa. *Sci. Adv.* **1**, e1500682 (2015).
140. Wainwright, C. M. et al. 'Eastern African paradox' rainfall decline due to shorter not less intense long rains. *npj Clim. Atmos. Sci.* **2**, 34 (2019).
141. Cai, W. et al. Projected response of the Indian Ocean Dipole to greenhouse warming. *Nat. Geosci.* **6**, 999–1007 (2013).
142. Cai, W. et al. Opposite response of strong and moderate positive Indian Ocean Dipole to global warming. *Nat. Clim. Change* **11**, 27–32 (2021).
143. Munday, C. & Washington, R. Controls on the diversity in climate model projections of early summer drying over southern Africa. *J. Clim.* **32**, 3707–3725 (2019).
144. Lazenby, M. & Todd, M. Evaluating future changes in the South Indian Ocean convergence zone projected by CMIP5 models and associated uncertainty. *Clim. Res.* **91**, 191–209 (2023).
145. Howard, E. & Washington, R. Tracing future spring and summer drying in southern Africa to tropical lows and the Congo air boundary. *J. Clim.* **33**, 6205–6228 (2020).

146. Cai, W. et al. Increased ENSO sea surface temperature variability under four IPCC emission scenarios. *Nat. Clim. Change* **12**, 228–231 (2022).
147. Crespo, L. R. et al. Weakening of the Atlantic Nino variability under global warming. *Nat. Clim. Change* **12**, 822–827 (2022).
148. Yang, Y. et al. Suppressed Atlantic Nino/Nina variability under greenhouse warming. *Nat. Clim. Change* **12**, 814–821 (2022).
149. Li, S. J. et al. The Pacific Decadal Oscillation less predictable under greenhouse warming. *Nat. Clim. Change* **10**, 30–34 (2020).
150. Li, G. & Xie, S. P. Tropical biases in CMIP5 multimodel ensemble: the excessive equatorial Pacific cold tongue and double ITCZ problems. *J. Clim.* **27**, 1765–1780 (2014).
151. Hirons, L. & Turner, A. The impact of Indian Ocean mean-state biases in climate models on the representation of the East African short rains. *J. Clim.* **31**, 6611–6631 (2018).
152. Jia, F. et al. Weakening Atlantic Nino–Pacific connection under greenhouse warming. *Sci. Adv.* **5**, eaax4111 (2019).
153. Wang, S. et al. El Niño/Southern Oscillation inhibited by submesoscale ocean eddies. *Nat. Geosci.* **15**, 112–117 (2022).
154. Giorgi, F., Jones, C. & Asrar, G. R. Addressing climate information needs at the regional level: the CORDEX framework. *WMO Bull.* **58**, 175–183 (2009).
155. Endris, H. S. et al. Assessment of the performance of CORDEX regional climate models in simulating East African rainfall. *J. Clim.* **26**, 8453–8475 (2013).
156. Engelbrecht, F. et al. Multi-scale climate modelling over southern Africa using a variable-resolution global model. *Water Sa* **37**, 647-658 (2011).
157. Dosio, A. & Panitz, H.-J. Climate change projections for CORDEX-Africa with COSMO-CLM regional climate model and differences with the driving global climate models. *Clim. Dyn.* **46**, 1599–1625 (2016).
158. Hong, S. Y. & Kanamitsu, M. Dynamical downscaling: fundamental issues from an NWP point of view and recommendations. *Asia-Pac. J. Atmos. Sci.* **50**, 83–104 (2014).
159. Geng, T., Cai, W., Jia, F. & Wu, L. Decreased ENSO post-2100 in response to formation of a permanent El Niño-like state under greenhouse warming. *Nat. Commun.* **15**, 5810 (2024).
160. Peng, Q., Xie, S.-P. & Deser, C. Collapsed upwelling projected to weaken ENSO under sustained warming beyond the twenty-first century. *Nat. Clim. Change* **14**, 815–822 (2024).
161. Funk, C. in *Drought, Flood, Fire: How Climate Change Contributes to Catastrophes* (ed. Funk, C. C.) 186–211 (Cambridge Univ. Press, 2021).
162. Hersbach, H. et al. The ERA5 global reanalysis. *Q. J. R. Meteorol. Soc.* **146**, 1999–2049 (2020).
163. Kalnay, E. et al. The NCEP/NCAR 40-year reanalysis project. *Bull. Am. Meteorol. Soc.* **77**, 437–472 (1996).
164. Schneider, U., Fuchs, T., Meyer-Christoffer, A. & Rudolf, B. GPCC's new land surface precipitation climatology based on quality-controlled in situ data and its role in quantifying the global water cycle. *Theor. Appl. Climatol.* **115**, 15–40 (2008).
165. Huang, B. et al. Extended reconstructed sea surface temperature, version 5 (ERSSTv5): upgrades, validations, and intercomparisons. *J. Clim.* **30**, 8179–8205 (2017).
166. Rayner, N. A. et al. Global analyses of sea surface temperature, sea ice, and night marine air temperature since the late nineteenth century. *J. Geophys. Res.* https://doi.org/10.1029/2002JD002670 (2003).
167. Huang, B. et al. Improvements of the Daily Optimum Interpolation Sea Surface Temperature (DOISST) version 2.1. *J. Clim.* **34**, 2923–2939 (2021).
168. Harris, I., Osborn, T. J., Jones, P. & Lister, D. Version 4 of the CRU TS monthly high-resolution gridded multivariate climate dataset. *Sci. Data* **7**, 109 (2020).
169. Reynolds, R. W., Rayner, N. A., Smith, T. M., Stokes, D. C. & Wang, W. An improved in situ and satellite SST analysis for climate. *J. Clim.* **15**, 1609–1625 (2002).
170. Henley, B. J. et al. A tripole index for the Interdecadal Pacific Oscillation. *Clim. Dyn.* **45**, 3077–3090 (2015).
171. Deser, C. & Phillips, A. S. Defining the internal component of Atlantic multidecadal variability in a changing climate. *Geophys. Res. Lett.* **48**, e2021GL095023 (2021).
172. Harrison, M. S. J. A generalized classification of South African summer rain-bearing synoptic systems. *J. Climatol.* **4**, 547–560 (1984).
173. Yang, W., Seager, R., Cane, M. A. & Lyon, B. The annual cycle of East African precipitation. *J. Clim.* **28**, 2385–2404 (2015).

Acknowledgements
The authors are grateful to J. Gan and the team from the Centre for Ocean Research, Hong Kong University of Science and Technology, for hosting the workshop on "Climate Variability and Impact on Africa" and for providing travel support. This project is supported by SKLLQGYS01. H.C.N was supported by Deutsche Forschungsgemeinschaft (DFG) grant 456490637. N.K. was supported by the research council of Norway (grant no. 328935). E.M. and B.R.-F. received funding from the Spanish Ministry of Science and Innovation projects (PID2021-125806NB-I00 and TED2021-130106B-I00). G.W., B.N., A.S.T. and X.Z. are supported by the Climate Systems Hub of the Australian Government's National Environment Science Program. S.L. was supported by the National Natural Science Foundation of China (NSFC) projects 42376198 and 42006173. PMEL contribution no. 5586. The authors acknowledge the World Climate Research Programme's Working Group on Coupled Modelling, which is responsible for CMIP, and they thank the climate modelling groups for producing and making available their model output, and the US Department of Energy Program for Climate Model Diagnosis and Intercomparison for coordinating support and leading development of software infrastructure in partnership with the Global Organization for Earth System Science Portals. The authors are grateful to various reanalysis groups for making the datasets available.

Author contributions
W.C. and M.J.M. conceived the article. The manuscript was written as a group effort through participation in several "Climate Impact on Africa" workshops held online and at Hong Kong University of Science and Technology. W.C. designed the article and coordinated the writing. A.S. synthesized workshop key points. J.M. led Box 1. C.R., E.M. and B.R.-F. led discussion and revision of content synthesized into the 'Dynamical connections of ENSO to Africa' and 'ENSO effects on the African climate' sections. W.C. led other sections. Xichen. L., B.N., Y.L. and T.G. performed analyses and created the figures. All authors contributed to the manuscript preparation, interpretation and discussions.

Competing interests
The authors declare no competing interests.

Additional information
Supplementary information The online version contains supplementary material available at https://doi.org/10.1038/s43017-025-00705-7.

Peer review information *Nature Reviews Earth & Environment* thanks Titike Bahaga and the other, anonymous, reviewer(s) for their contribution to the peer review of this work.

[1]State Key Laboratory of Physical Oceanography/Frontiers Science Center for Deep Ocean Multispheres and Earth System/Sanya Oceanographic Institution, Ocean University of China, Qingdao, China. [2]State Key Laboratory of Loess Science, Institute of Earth Environment, Chinese Academy of Sciences, Xi'an, China. [3]Laoshan Laboratory, Qingdao, China. [4]Department of Oceanography, University of Cape Town, Cape Town, South Africa. [5]Departamento de Física de la Tierra y Astrofísica, Universidad Complutense de Madrid, Madrid, Spain. [6]Instituto de Geociencias, IGEO (UCM-CSIC), Madrid, Spain. [7]Agricultural Research Council-Natural Resources and Engineering, Pretoria, South Africa. [8]CLIVAR International Project Office, Qingdao, China. [9]Climate Change Research Centre (CCRC), University of New South Wales, Sydney, New South Wales, Australia. [10]Institute of Atmospheric Physics, Chinese Academy of Sciences, Beijing, China. [11]Institute of Ocean Research, Peking Unviersity, Beijing, China. [12]Department of Geography and Environmental Studies, University of Limpopo, Mankweng, South Africa. [13]GEOMAR Helmholtz Centre for Ocean Research Kiel, Kiel, Germany. [14]Department of Geography, University of Nigeria, Nsukka, Nigeria. [15]NOAA/Pacific Marine Environmental Laboratory, Seattle, WA, USA. [16]Geophysical Institute, University of Bergen, Bergen, Norway. [17]Bjerknes Centre for Climate Research, University of Bergen, Bergen, Norway. [18]Nansen Environmental and Remote Sensing Centre, Bergen, Norway. [19]Nansen-Tutu Centre for Marine Environmental Research, Department of Oceanography, University of Cape Town, South Africa, South Africa. [20]ARC Centre of Excellence for Climate Extremes, University of New South Wales, Sydney, New South Wales, Australia. [21]ARC Centre of Excellence for the Weather of the 21st Century, University of New South Wales, Sydney, New South Wales, Australia. [22]CSIRO Environment, Hobart, Tasmania, Australia. [23]Key Laboratory of Ocean Circulation and Waves, Institute of Oceanology, Chinese Academy of Sciences, Qingdao, China. [24]College of Global Change and Earth System Science, Beijing Normal University, Beijing, China. [25]Department of Physics, University of Yaounde, Yaounde, Cameroon. [26]Department of Atmospheric and Environmental Sciences, University at Albany, State University of New York (SUNY), Albany, NY, USA. [27]Global Change Institute, University of the Witwatersrand, Johannesburg, South Africa. [28]Department of Environmental Studies, New York University, New York, NY, USA. [29]University of Nairobi, Nairobi, Kenya.